1   # Kinetics of H_2-O_2-H_2O redox equilibria and formation of metastable H_2O_2

2   ## under low temperature hydrothermal conditions

3

4   Dionysis I. Foustoukos[1*], Jennifer L. Houghton[2] , William E. Jr. Seyfried[3], Stefan M.
5   Sievert[4] and George D. Cody[1]

6

7   *[1]Geophysical Laboratory, Carnegie Institution of Washington, 5251 Broad Branch Rd. NW,*
8   *Washington DC 20015*

9

10   *[2]Environmental Science Program, Rhodes College, Memphis,TN 38112*

11

12   *[3]Department of Geology, University of Minnesota, 310 Pillsbury Drive SE, Minneapolis, MN*
13   *55455*

14

15   *[4] Department of Biology, Woods Hole Oceanographic Institution, Woods Hole, MA 02543*

16

17   *Correspondence author: dfoustoukos@ciw.edu*

18

19   Keywords: Knallgas reaction, H_2 oxidation, metastable hydrogen peroxide, anaerobic

20   chemolithoautotrophic metabolism, Fenton reaction, hydrothermal systems

21

22   Running Title: Kinetics of H_2-O_2-H_2O equilibria and formation of metastable H_2O_2

23

24

ABSTRACT

Hydrothermal experiments were conducted to evaluate the kinetics of $H_{2(aq)}$ oxidation in the homogeneous H_2-O_2-H_2O system at conditions reflecting subsurface/near-seafloor hydrothermal environments (55-250 ^{o}C and 242-497 bar). The kinetics of the water-forming reaction that controls the fundamental equilibrium between dissolved $H_{2(aq)}$ and $O_{2(aq)}$, are expected to impose significant constraints on the redox gradients that develop when mixing occurs between oxygenated seawater and high-temperature anoxic vent fluid at near-seafloor conditions. Experimental data indicate that, indeed, the kinetics of $H_{2(aq)}$-$O_{2(aq)}$ equilibrium become slower with decreasing temperature, allowing excess $H_{2(aq)}$ to remain in solution. Sluggish reaction rates of $H_{2(aq)}$ oxidation suggest that active microbial populations in near-seafloor and subsurface environments could potentially utilize both $H_{2(aq)}$ and $O_{2(aq)}$, even at temperatures lower than 40 ^{o}C due to $H_{2(aq)}$ persistence in the seawater/vent fluid mixtures. For these H_2-O_2 disequilibrium conditions, redox gradients along the seawater/hydrothermal fluid mixing interface are not sharp and microbially-mediated $H_{2(aq)}$ oxidation coupled with a lack of other electron acceptors (e.g. nitrate) could provide an important energy source available at low-temperature diffuse flow vent sites.

More importantly, when $H_{2(aq)}$-$O_{2(aq)}$ disequilibrium conditions apply, formation of metastable hydrogen peroxide is observed. The yield of $H_2O_{2(aq)}$ synthesis appears to be enhanced under conditions of elevated $H_{2(aq)}/O_{2(aq)}$ molar ratios that correspond to abundant $H_{2(aq)}$ concentrations. Formation of metastable H_2O_2 is expected to affect the distribution of dissolved organic carbon (DOC) owing to the existence of an additional strong oxidizing agent. Oxidation of magnetite and/or Fe^{++} by hydrogen peroxide could also induce formation of metastable hydroxyl radicals ($\bullet$OH) through Fenton-type

49   reactions, further broadening the implications of hydrogen peroxide in hydrothermal

50   environments.

1. Introduction

Low-temperature diffuse fluid flow in submarine hydrothermal systems represents an important mechanism of heat and mass transfer in mid-ocean ridges, playing a key role in the re-distribution of volatiles and metals. In general, diffuse flow systems involve subseafloor mixing between oxygenated cold seawater and high-temperature anoxic hydrothermal fluid (CORLISS et al., 1979; EDMOND et al., 1979). The contrasting chemical and physical conditions of these two fluid sources induce sharp gradients, with important implications for the distribution of redox- and pH-sensitive aqueous species (DING et al., 2001; DING et al., 2005; KELLEY et al., 2002; LUTHER et al., 2001; TIVEY, 1995). Identifying metastable equilibria that likely accompany redox and pH gradients not only helps to elucidate subseafloor hydrothermal alteration processes, but may also contribute important insights into the nature of energy sources fueling a subseafloor biosphere. For example, availability of dissolved oxygen, a major source of metabolic energy for aerobic lithoautotrophs, in the presence of reduced inorganic compounds, influences the distribution of aerobic and anaerobic bacteria in the subsurface (EDWARDS et al., 2005; REYSENBACH and SHOCK, 2002). The existence of hydrogen-utilizing chemolithotrophic bacteria in chimney structures, however, is also consistent with the persistence of $H_{2(aq)}$-enriched fluids at low temperatures (T < 70 ^{o}C) (REYSENBACH et al., 2000).

The distribution of redox couples (e.g. $H_{2(aq)}/O_{2(aq)}$, $H_2S_{(aq)}/SO_4^{--}$) is typically assessed by use of geochemical mixing models constructed assuming complete thermodynamic equilibria or complete disequilibria (MCCOLLOM and SHOCK, 1997; SHOCK and HOLLAND, 2004). A number of experimental and field studies, however, have suggested that these assumptions might be invalid, especially for moderately low

74 temperatures (< 200 ^{o}C) (DING et al., 2001; FOUSTOUKOS et al., 2009; MCCOLLOM and

75 SEEWALD, 2006). For example, fluid samples collected from diffuse and focused flow

76 vents at the Main Endeavour Field (MEF) along Juan de Fuca Ridge indicate that the

77 types of organic species can be related to the geochemical processes occurring within the

78 seawater-hydrothermal fluid mixing zone (FOUSTOUKOS et al., 2009). In particular, the

79 distribution of dissolved volatiles measured in the high and low-temperature

80 hydrothermal vent fluids at MEF confirms the strong effect of temperature on the kinetics

81 of the CO_2-CO-H_2-H_2O redox equilibria (SEEWALD et al., 2006), where slow CO_2-CO

82 reaction rates are indicated at temperatures less than 50 ^{o}C.

83   Another important redox couple that can be linked to subsurface mixing processes

84 involves dissolved $H_{2(aq)}$ and $O_{2(aq)}$ species. Theoretical studies have suggested that $H_{2(aq)}$-

85 $O_{2(aq)}$ disequilibrium can provide large energy sources to support microbial metabolism in

86 deep-sea vent environments (MCCOLLOM and SHOCK, 1997; SHOCK and HOLLAND,

87 2004). At elevated temperature and pressure (350 ^{o}C-350 bar), the water-forming reaction

88 that ultimately constrains this redox couple has been shown to achieve thermodynamic

89 equilibrium rapidly (SEEWALD, 1994). However, at low temperatures only one set of

90 experimental data exists (Table 1) (HOUGHTON, 2003). These data describe $H_{2(aq)}$

91 oxidation rates at 100 ^{o}C-500 bar in the homogeneous H_2-O_2-H_2O system and support the

92 presence of excess $H_{2(aq)}$ in solution after mixing $H_{2(aq)}$- and $O_{2(aq)}$-enriched aqueous

93 fluids (Table 1). Furthermore, $H_{2(aq)}$-$O_{2(aq)}$ disequilbrium at low temperatures (< 37 ^{o}C)

94 has also been suggested by dissolved oxygen concentrations measured in groundwaters

95 and in experimental studies involving pyrite oxidation (KAMEI and OHMOTO, 2000;

96 LINDBERG and RUNNELLS, 1984), where aqueous solutions maintained elevated $O_{2(aq)}$

97   concentrations even at highly reducing conditions. Thus, to more closely examine the

98   effect of temperature on $H_{2(aq)}$-$O_{2(aq)}$ equilibrium, a series of hydrothermal experiments

99   were conducted in the homogeneous H_2-O_2-H_2O system, at temperature and pressure

100 conditions reflecting subsurface/near-seafloor hydrothermal environments (55-250 ^{o}C

101 and 242-497 bar). This study also examines the formation of metastable aqueous species.

102 For example, reducing conditions when coupled with disequilibrium between dissolved

103 oxygen and hydrogen, could contribute to the formation of metastable aqueous oxidants

104 (e.g. $H_2O_{2(aq)}$). The formation of such as species could affect redox gradients developed

105 within the seawater-hydrothermal fluid mixing zone with implications not only for the

106 chemical evolution of diffuse flow hydrothermal fluids, but also for the diversity of the

107 near-vent microbial and macrofaunal communities.

108

109 **2. Methods**

110 **2.1 Experimental and Analytical Procedures**

111   To determine $H_{2(aq)}$ oxidation rates at a wide range of temperatures (55-250 ^{o}C),

112 hydrothermal experiments were conducted by using both "open system" flow-through

113 (Geophysical Lab) and "closed system" batch reactors (University of Minnesota) (Table

114 3, 4). The batch reactor system facilitated determination of equilibrium phase relations,

115 while the flow-though experiments were better suited to assess reaction rates. In effect, a

116 60 ml flexible Au/Ti cell reaction cell was used to overcome "open system" limitations

117 linked to short reaction times. For example, in the flow-through experimental system,

118 fluid flow rates were adjusted to provide residence times up to 15 minutes. Reaction

119 times up to 1451 minutes were achieved in the flexible Au/Ti cell (Table 3, 4). The latter

120   experimental design allows time series sampling of internally filtered fluid at

121   experimental conditions (SEYFRIED et al., 1987), while the chemical composition of the

122   reactant fluids can be modified at any time by "in-situ" injection of aqueous solutions

123   directly in the cell through a sampling valve. Thus, the progress of the H_2-O_2 redox

124   equilibrium can be monitored and controlled. However, to evaluate reaction kinetics that

125   exhibit short half-life (e.g. few minutes) use of the flow-through design is more

126   appropriate. In the flow-through experiments, a fixed volume (3.251 ml) cylindrical

127   titanium reactor was placed into a gravity-convection Lindberg/Blue oven with

128   temperatures uniformity of 4 ^{o}C at 200 ^{o}C. Aqueous solutions were delivered by a high

129   precision dual-cylinder and gas-tight titanium pump (Quizix SP5000) that provides

130   continuous and pulse-free fluid flow at a constant flow rate. The residence time of the

131   reactant fluids in the cell was controlled by adjusting the flow rate of fluid delivery,

132   which was maintained under constant pressure conditions by an inline backpressure

133   regulator (Coretest DBPR-5). A similar design was adopted by Foustoukos et al. (2007)

134   to evaluate the distribution of trace elements within the two phase region of the NaCl-

135   H_2O system at elevated temperatures and pressures.

136   In all experiments, dissolved $O_{2(aq)}$ was produced by complete thermal

137   decomposition of dilute $H_2O_{2(aq)}$ aqueous solutions (Sigma-Aldrich), with known starting

138   composition (Table 3, 4). Dissolved H_2 was introduced either by direct injection into the

139   flexible Au/Ti cell, or by purging the reactant solution with H_2 gas at atmospheric

140   pressures prior to delivery by the gas-tight Quizix 5000 pump. Dissolved volatile

141   concentrations were adjusted to reflect the compositional variability expected at near-vent

142   mixing hydrothermal environments. Furthermore, to estimate final mixing ratios needed

143 to properly evaluate the chemical composition of the solution mixture in the batch

144 reactor, the $H_{2(aq)}$-bearing fluids were spiked with 176 ppm of Cl, which served as a

145 conservative chemical tracer. Fluid samples were collected in gas-tight Hamilton locking

146 syringes and then analyzed for dissolved $H_{2(aq)}$, $O_{2(aq)}$ and $N_{2(aq)}$ by a SRI 8610C gas

147 chromatograph equipped with TCD detector and a Carboxen-1010 Plot/Silica-Gel

148 column. Analytical errors are within 5% (2σ) and reflect the larger values of errors

149 between instrument calibration and duplicate analysis of individual samples. Nitrogen

150 concentrations were monitored to account for the atmospheric O_2 contributions

151 introduced during sampling and to adjust accordingly the measured $O_{2(aq)}$ concentrations.

152 Data collected are indicative of minimal air contamination corresponding to very low N_2

153 concentrations (0.2 – 2.7 %). Dissolved chloride concentrations were measured by ion

154 chromatography with estimated uncertainties (2σ) of less than 2%. Fluid pH was

155 measured with a glass combination Thermo-Orion Micro-pH electrode coupled with an

156 Orion Benchtop 250 A pH/mV meter.

157

158   **2.2 Analytical methodology for $H_2O_{2(aq)}$**

159   Dissolved $H_2O_{2(aq)}$ concentrations were retrieved by a Labsystem Multiskan

160 MCC/340 MKII spectrophotometer, following the fluorometric Amplex Red

161 methodology (A-22188 Molecular Probes) with detection limits as low as 50 nmol/kg

162 (ZHOU et al., 1997). This technique involves reaction of H_2O_2 with the Amplex Red

163 reagent (1:1 stoichiometry) and formation of highly fluorescent resorufin under the

164 presence of horseradish peroxidase. The main advantage of the Amplex Red is the low

165 background fluorescence and the enhanced stability of produced resorufin (GOMES et al.,

166 2005, and references therein). A number of studies have shown that Amplex Red is a

167 sensitive and specific probe for the detection of H_2O_2 (COHN et al., 2008;

168 GYULKHANDANYAN and PENNEFATHER, 2004; SEAVER and IMLAY, 2001; SEAVER and

169 IMLAY, 2004).

170 To further establish the accuracy of analytical techniques for hydrogen peroxide

171 detection, a series of flow-through experiments was performed to investigate the kinetics

172 of $H_2O_{2(aq)}$ decomposition in the homogeneous H_2O-$H_2O_{2(aq)}$ system, at temperatures and

173 pressures typical of seafloor mixing hydrothermal environments (60 - 200 ^{o}C, 242 bar)

174 (Table 2). In general, the complete decomposition of $H_2O_{2(aq)}$ is assumed to follow first-

175 order reaction kinetics in keeping with previous studies (CROISET et al., 1997; HIROKI et

176 al., 2002; LIN et al., 1991) and described as:

$$H_2O_{2(aq)} \rightarrow H_2O + \tfrac{1}{2} O_{2(aq)} \tag{1}$$
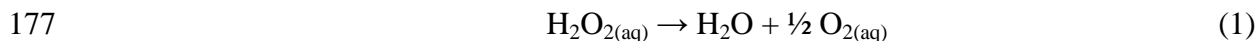
$$-\frac{d[H_2O_2]}{dt} = k_{H_2O_2}[H_2O_2] \tag{2}$$

179 where k_{H2O2} is the observed decomposition rate coefficient in s^{-1} and t is time in seconds.

180 Results confirm a first-order reaction rate, exhibiting a strong linear correlation between

181 the natural logarithm of $H_2O_{2(aq)}$ concentrations and reaction time giving a slope that

182 defines the k_{H2O2} at each temperature (Fig. 1a). The temperature-dependent decay rate can

183 then be expressed by the Arrhenius equation:

$$\ln(k_{H_2O_2}) = \ln(A) - \frac{E_a}{RT} \tag{3}$$

185 where E_a is the activation energy, A is the pre-exponential (or frequency) factor, R is the

186 gas constant (8.314 J mol^{-1} K^{-1}) and T is temperature in Kelvin. The linear temperature

187 dependence of observed k_{H2O2} is in good agreement with previously published data (Fig.

188 1b) (CROISET et al., 1997; LIN et al., 1991), supporting the applicability of experimental

189 and analytical protocols used in this study. The estimated activation energy of 45.1

190 kJ/mole and the pre-exponential factor of 728 s^{-1}, strictly apply to the titanium-bearing

191 flow-through system utilized, but these values are in good agreement with similar data

192 from other studies in which inconel 625 reactors were utilized. In general, reactor surface

193 effects are linked to the oxidation potential of the material and the catalytically enhanced

194 stability of intermediate OH and HO$_2$ radicals in the H$_2$O$_2$ decomposition scheme (HART

195 et al., 1963; HOARE et al., 1967; LIN et al., 1991; TAKAGI and ISHIGURE, 1985). These

196 short-lived radicals would remain absorbed on the metallic surface and likely affect their

197 reactivity potential towards H$_2$O$_{2(aq)}$ decomposition (LIN et al., 1991). Overall, our results

198 indicate a decrease of the half-life (0.693/ k_{H2O2}) of H$_2$O$_{2(aq)}$ from 200 min at 60 ^{o}C to 2

199 min at 200 ^{o}C, revealing a clear inverse effect of temperature on H$_2$O$_2$ stability.

200

201 **3. Results**

202 A total of 6 hydrothermal experiments were performed to assess temperature

203 effects on the rate of the H$_{2(aq)}$-O$_{2(aq)}$ equilibrium at pressures applicable to near-seafloor

204 hydrothermal systems (242-497 bar) (Table 3,4). This redox equilibrium can be

205 expressed by the so-called Knallgas reaction:

206 $$H_{2(aq)} + \tfrac{1}{2} O_{2(aq)} \rightarrow H_2O \tag{4}$$
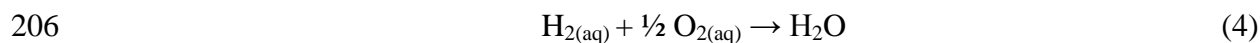
207 It is expected that reaction (4) obeys first-order reaction kinetics with respect to H$_{2(aq)}$

208 abundances, as follows:

209 $$-\frac{d[H_2]}{dt} = k_{H_2}[H_2] \tag{5}$$

210   where k_{H2} is the decomposition rate coefficient in s^{-1} and t is time in seconds. Data

211   obtained exhibit a strong linear correlation ($r^2 = 0.89$-0.99) between reaction time and the

212   natural logarithm of the $H_{2(aq)}$ concentrations measured in solution, indicative of a first-

213   order reaction mechanism (Table 3, 4).

214   In general, results from the flow-through experiments indicate a nearly 39%

215   decrease of dissolved $H_{2(aq)}$ concentrations at 250 ^{o}C within the first 5 minutes of the

216   reaction, consistent with rapid $H_{2(aq)}$-$O_{2(aq)}$ equilibration. Estimated kinetic rate constants

217   at 200 ^{o}C and 250 ^{o}C are 4.11 x 10^{-4} to 5.35 x 10^{-4} s^{-1}, respectively (Table 3, Fig. 2a), and

218   only an order of magnitude slower than the rates of hydrogen peroxide decomposition

219   (Fig. 1b). Thus, at these elevated temperature conditions, trace amounts of $H_2O_{2(aq)}$ may

220   have persisted during the very early stages of reaction with minimal effect on the overall

221   H_2 oxidation process..

222   Rate constants of the H_2-O_2 equilibrium decreased with decreasing temperatures,

223   ranging from 1.89 x 10^{-4} to 2.69 x 10^{-5} s^{-1} at 125 ^{o}C and 55 ^{o}C respectively, consistent

224   with the abundance of dissolved $H_{2(aq)}$ concentrations, even after several hours of reaction

225   (Table 4). In effect, the first order temperature-dependent rate of $H_{2(aq)}$ oxidation can be

226   described with an activation energy (E_a) of 24 $\pm$ 3.4 kJ/mole, and an pre-exponential

227   factor (A) of 6.7 $\pm$ 6.7 s^{-1}. Reaction half-life ranges from 22 minutes to 430 minutes at

228   250 ^{o}C and 55 ^{o}C respectively (Fig. 2).

229   The relatively high $H_{2(aq)}$ concentrations in these experiments are accompanied by

230   formation of metastable hydrogen peroxide. In fact, dissolved $H_2O_{2(aq)}$ concentrations

231   reached values (0.002 – 0.156 mmol/kg), and persisted in solution for significantly longer

232   reaction times that those predicted from H_2O_2 decomposition rates for the pure H_2O_2-H_2O

233   system (Fig. 1b). These observations appear to indicate involvement of both $H_{2(aq)}$ and

234    $O_{2(aq)}$ in solution on rate relations (Table 4). Elevated $H_{2(aq)}/O_{2(aq)}$ molar ratios and high

235    $H_{2(aq)}$, concentrations enhance the stability of $H_2O_{2(aq)}$ even at temperatures as high as

236    $125^{\circ}C$. These results are in agreement with previous studies, where comparable amounts

237   of $H_2O_{2(aq)}$ were produced at $100\ ^{\circ}C$ - 500 bars, under similar compositional constraints

238   (e.g. species concentrations, H_2/O_2 molar ratios) (Table 1) (HOUGHTON, 2003). The fact

239   that hydrothermal formation of hydrogen peroxide is viable at these temperatures and

240   pressures suggests that this species needs to be considered at deep-sea vents. In effect,

241   such enrichments of strong oxidants might inhibit the growth of microbial communities,

242   while the relative distribution of dissolved $H_{2(aq)}$ and $O_{2(aq)}$ could affect the extent of

243   aerobic and anaerobic microbial habitats by defining redox gradients in the near-seafloor

244   hydrothermal vents (EDWARDS et al., 2005; REYSENBACH and SHOCK, 2002).

245

246   **4. Discussion**

247   **4.1 The role of H_2-O_2-H_2O redox equilibria on habitability**

248   The H_2-O_2-H_2O disequilibria observed in this study adds to the distribution of

249   reductants/oxidants in seafloor hydrothermal systems (e.g. $H_{2(aq)}/O_{2(aq)}$, $H_2S_{(aq)}/SO_4^{--}$,

250   Fe^{++}/Fe^{+++}), as well as the overall energy available to microorganisms (MCCOLLOM and

251   SHOCK, 1997). Early models assumed instantaneous equilibration between $H_{2(aq)}$ and

252    $O_{2(aq)}$ and predict an abrupt transition between oxic and anoxic conditions, corresponding

253   to the distribution of redox species in the vent fluid/seawater mixture and the Gibbs (ΔG_r)

254   energy for each redox reaction. Later models recognized the importance of the

255   dependence of the oxic/anoxic interface on the relative abundance of $H_{2(aq)}$ and $O_{2(aq)}$ in

256 evolved mixture solutions (SHOCK and HOLLAND, 2004). Thus, experimental data

257 demonstrating inhibition of the Knallgas reaction at low temperatures ($<150\ ^oC$) will

258 greatly affect the spatial extent of both aerobic and anaerobic bacterial populations in

259 near-seafloor habitats. In fact, the existence of both (hyper)thermophilic and mesophilic

260 hydrogen-oxidizing bacteria utilizing O_2, NO_3^-, and/or S^0 as electron acceptors has been

261 observed in chimney structures and near-vent diffuse flow sites (CAMPBELL et al., 2006;

262 NAKAGAWA and TAKAI, 2008; REYSENBACH and SHOCK, 2002).

263   Aerobic and anaerobic chemolithoautotrophic microorganisms that thrive in the

264 mixing zone between reducing hydrothermal fluid and oxygenated seawater are highly

265 abundant in a variety of mid-ocean ridge hydrothermal systems. In particular bacteria

266 belonging to the *Epsilonproteobacteria* and *Aquificales* play an important role as primary

267 producers at deep-sea hydrothermal vents (CAMPBELL et al., 2006; NAKAGAWA and

268 TAKAI, 2008; REYSENBACH and SHOCK, 2002). Both groups exhibit similar metabolisms

269 – i.e. the oxidation of reduced sulfur compounds and hydrogen with both oxygen and

270 nitrate or the oxidation of hydrogen with elemental sulfur coupled to the fixation of

271 inorganic carbon – and thus occupy a similar ecological niche. However, they seem to be

272 partitioned by their temperature preference, with *Epsilonproteobacteria* dominating the

273 microbial communities at temperatures from 20 °C to 60 °C, whereas *Aquificae* seem to

274 be the predominant autotrophs at temperatures higher than 60 °C (CAMPBELL et al., 2006;

275 NAKAGAWA and TAKAI, 2008). Different groups of *Epsilonproteobacteria* might also

276 occupy different niches. Members of the *Nautilia/Caminibacter* group grow at

277 temperatures between 40 °C and 70 °C, and they rely on hydrogen oxidation coupled to

278 S^0- or nitrate reduction (to NH_4^+) as their energy source. In contrast, members of the

279 *Sulfurimonas* group or the *Sulfurovum* group grow at lower temperatures between 10 °C

280 and 40 °C, and use reduced sulfur compounds and/or molecular hydrogen as electron

281 donors and oxygen or nitrate (to N_2) as electron acceptors (CAMPBELL et al., 2006).

282 Compared to other epsilonproteobacterial isolates, members of these groups can tolerate

283 relatively high amounts of oxygen (NAKAGAWA and TAKAI, 2008); metabolic features

284 that might be beneficial in ecosystems where intensive mixing of hydrothermal fluids and

285 seawater takes place.

286　　　　To better understand the spatial extent of the H_2-O_2 gradient in near-seafloor

287 hydrothermal mixing zones, thermodynamic calculations in the homogeneous H_2-O_2-H_2O

288 system were performed utilizing the experimentally derived kinetic rate law constants (*A*,

289 E_a), while assuming first-order reaction kinetics for the H_2-O_2 redox equilibrium. The

290 reaction path calculations were modeled with Geochemist's Workbench (BETHKE, 1996;

291 BETHKE, 2002), making use of compositional constraints on both seawater and

292 hydrothermal fluid as described by McCollom and Shock (1997). Concentrations of

293 dissolved H_2 for the hydrothermal fluid are lower (1.3 mmol/kg) than in the previous

294 models (1.7 mmol/kgl), accounting for the lack of other competitive oxidation reaction

295 involving Fe^{+2}, $H_2S_{(aq)}$, S^o or Mn^{+2}. Results suggest the presence of a sharp redox gradient

296 at 38 ^{o}C once conditions reach equilibria (Fig. 3). However, short-term mixing processes

297 allow fluids to achieve simultaneous enrichment in both $H_{2(aq)}$ and $O_{2(aq)}$. For example,

298 even after 10 hours of homogeneous mixing at temperatures as low as 20 ^{o}C, diffuse flow

299 fluids retain micromolar concentrations of H_2, while shorter reaction times permit more

300 reducing conditions and possibly the establishment of anaerobic zones. Similarly,

301 persistence of dissolved $O_{2(aq)}$ at temperatures higher than 38 ^{o}C (Fig. 3) could promote

302 growth of microaerophilic chemolithoautotrophs, such as *Aquificaceae and*

303 *Hydrogenothermaceae (e.g. Aquificales)* which grow between 60 °C and 90 °C

304 (NAKAGAWA and TAKAI, 2008).

305

306 *4.1.1 An example: H_2-O_2-H_2O disequilibria and the metabolic pathways of the anaerobic*

307 *nitrate reducers*

308   Biological reduction of dissolved NO_3^- is well known to proceed either through

309 denitrification (i.e. formation of N_2) or ammonification (i.e formation of NH_4^+). In near-

310 seafloor hydrothermal environments, mixing between deep water and high-temperature

311 hydrothermal fluid results in diffuse flow fluids being enriched in NO_3^- (20 - 40 μM in

312 seawater SCHLITZER, 2000) while maintaining moderately high $H_{2(aq)}$ concentrations in

313 accordance with the sluggish kinetics of H_2-O_2 redox equilibrium (Fig. 2). For example,

314 both processes have been suggested to occur at Axial Volcano, Juan de Fuca Ridge,

315 where dissolved NO_3^- concentrations of diffuse flow fluids exhibit depletion from values

316 expected for conservative mixing between seawater and hot hydrothermal fluids, while

317 accompanied by elevated concentrations of ammonia and the presence of nitrous oxide

318 and nitrite (BUTTERFIELD et al., 2004). In line with this observation, a number of

319 mesophilic and thermophilic *Epsilonproteobacteria* and *Aquificales* that perform either

320 denitrification or nitrate ammonification have been isolated from chimney structures and

321 diffuse-flow sites along mid-ocean ridges (ALAIN et al., 2002; GOTZ et al., 2002;

322 MIROSHNICHENKO et al., 2004; NAKAGAWA et al., 2005a; NAKAGAWA et al., 2003;

323 NAKAGAWA et al., 2005b; TAKAI et al., 2004; TAKAI et al., 2006; VETRIANI et al., 2004;

324 VOORDECKERS et al., 2008). Energetically both pathways exhibit similar potential to

325 support chemolithoautotrophic metabolism (STROHM et al., 2007). Denitrification,

326 however, has been shown to proceed under microaerobic conditions despite the

327 potentially inhibiting role of $O_{2(aq)}$ on anaerobic denitrifying activity (DAVIES et al., 1989;

328 HERNANDEZ and ROWE, 1987; MCKENNEY et al., 2001).

329   Overall, the range of $O_{2(aq)}$ concentrations that anaerobic NO_3^- reducers can

330 tolerate spans between 2 and 54 μM (GOTZ et al., 2002; NAKAGAWA et al., 2003;

331 NAKAGAWA et al., 2005b; TAKAI et al., 2004; TAKAI et al., 2006). These concentrations

332 would reflect important fractions of seawater (100 - 250 μM $O_{2(aq)}$ SCHLITZER, 2000) in

333 the low-temperature diffuse flow fluids and would contribute to strong redox gradients

334 along the mixing interface. Thermodynamic calculations on the energetic contributions of

335 the excess dissolved $O_{2(aq)}$ to the Knallgas reaction performed at 70 ^{o}C - 250 bars suggest

336 that it is the strongly out-of equilibrium $O_{2(aq)}$ concentrations that would account for most

337 of the bioavailable energy and not the concentration of dissolved $H_{2(aq)}$, even when the

338 latter ranges from 100 μM to 10 mM (Fig. 4). Thus, the tendency of denitrifiers to switch

339 between aerobic and anaerobic metabolism and to carry out nitrate reduction in the

340 presence of $O_{2(aq)}$ likely imposes an important constraint on microbial diversity at near-

341 seafloor hydrothermal sites as they can out compete organisms executing ammonification

342 under these conditions. On the other hand, under low nitrate concentrations, such as

343 expected at higher temperatures (i.e. elevated contribution of hydrothermal fluid in

344 diffuse flow), nitrate ammonification has been found to allow a higher growth yield than

345 denitrification (STROHM et al., 2007). Consequently, one could expect that organisms

346 carrying out ammonification have a competitive advantage under these conditions.

347 Currently, no conclusive data on the relative abundance of denitrifiers and ammonifiers at

348   different temperatures exist, but existing data on cultures are generally supportive of this

349   trend (CAMPBELL et al., 2006).

350

351   **4.2 Formation of metastable $H_2O_{2(aq)}$**

352   A number of studies have focused on the formation of hydrogen peroxide in

353   aqueous solutions through different reaction mechanisms. For example in Borda et al.

354   (2003), addition of pyrite grains to O_2-free water appeared to enhance adsorption of H_2O

355   and ferric Fe at sulfur-deficient lattice sites resulting in the possible formation of

356   metastable hydroxyl radicals and $H_2O_{2(aq)}$. Similarly, by applying mechanical or electric

357   charge stresses in silicate minerals, O_2-defect lattice sites bearing O^- species might be

358   formed, leading to oxidation of H_2O to H_2O_2 through formation of O radicals (BALK et

359   al., 2009; HUROWITZ et al., 2007). In addition, direct formation of $H_2O_{2(aq)}$ through $H_{2(aq)}$

360   oxidation by dissolved O_2 is promoted in the presence of Pd or Au-Pd supported catalyst

361   (T < 25 ^{o}C) (CHINTA and LUNSFORD, 2004; DISSANAYAKE and LUNSFORD, 2002;

362   DISSANAYAKE and LUNSFORD, 2003; EDWARDS et al., 2009; LANDON et al., 2003;

363   LUNSFORD, 2003; POSPELOVA et al., 1961). Reaction pathways that lead to direct $H_2O_{2(aq)}$

364   formation involve the hydrogenation of oxygen and H_2 activation to form an HO_2 surface

365   intermediate, with H_2O_2 decomposition to H_2O being inhibited, especially when

366   dissolved halides are in solution (Cl^-, Br^-, F^-, I^-) (EDWARDS et al., 2008; LUNSFORD, 2003;

367   POSPELOVA and KOBOZEV, 1961). Dissolved halides minimize the rate of H_2O_2

368   decomposition by changing the electronic properties of the catalyst and by eliminating

369   active lattice sites (CHOUDHARY and SAMANTA, 2006; CHOUDHARY et al., 2007). Thus, in

370   the homogeneous H_2-O_2-H_2O system of our study, the trace amounts of dissolved Cl^-

371 used as chemical tracer likely had little effect on the yield of hydrogen peroxide

372 synthesis. In deep sea hydrothermal environments, however, circulation of evolved

373 seawater might play a role in enhancing the stability of hydrogen peroxide possibly

374 formed in near-seafloor mixing zones. Likewise the surface of the Au/Ti reaction cell did

375 not affect reactions, as native Au has been shown to be chemically inert (HAN et al.,

376 2007), with TiO_2 exhibiting minimal effects on $H_2O_{2(aq)}$ decomposition (HIROKI et al.,

377 2002; LIN et al., 1991).

378   In our study, synthesis of metastable $H_2O_{2(aq)}$ occurred at low temperature

379 hydrothermal conditions (T < 150 ^{o}C) and in the absence of mineral or metal catalytic

380 surfaces. The stability of H_2O_2 appears to be associated with the availability of both $H_{2(aq)}$

381 and $O_{2(aq)}$ in solution, further supporting the role of H_2-O_2 redox disequilibrium in

382 promoting synthesis of metastable oxidants. In effect, concentrations of H_2O_2 attained

383 were significantly higher than those expected based on the kinetic rate of direct H_2O_2

384 decomposition and maintained constant along extensive reaction times (~ hrs) (Fig. 5)

385 (Table 4). Elevated $H_{2(aq)}/O_{2(aq)}$ molar ratios and high $H_{2(aq)}$ concentrations enhance

386 $H_2O_{2(aq)}$ formation, even at temperatures as high as 130°C (Fig. 5), suggesting that

387 conditions of elevated reduction potential might be required to facilitate synthesis of

388 strong oxidants. This is consistent with previous studies proposing that $H_{2(aq)}/O_{2(aq)}$ molar

389 ratios might play a role in controlling the relative rates of the two competing reaction

390 pathways of interest: H_2 oxidation to H_2O and/or H_2O_2 (CHINTA and LUNSFORD, 2004).

391 In this reaction scheme, hydrogen peroxide is considered an intermediate/metastable

392 phase towards water formation, and thus, it requires presence of both $H_{2(aq)}$ and $O_{2(aq)}$. In

393 effect, synthesis of $H_2O_{2(aq)}$ has been described as a hydrogenation reaction of O_2 to

394 account for the stability of the O-O relative to the weak H-H bonds (EDWARDS et al.,

395 2008).

396   Evidence for the catalytic effects of the elevated $H_{2(aq)}/O_{2(aq)}$ ratios provides an

397 explanation of the existence of dissolved H_2O_2 in the 95 ^{o}C experiment. For example,

398 $H_{2(aq)}$ injection after nearly 24 hrs of reaction resulted in a significant increase of $H_2O_{2(aq)}$,

399 the concentration of which eventually decreased following the gradual removal of $O_{2(aq)}$

400 through $H_{2(aq)}$ oxidation (Fig. 6). Accordingly H_2O_2 decomposition through

401 hydrogenation to H_2O ($H_{2(aq)}$ + $H_2O_{2(aq)}$ $\rightarrow$ H_2O) is kinetically favored over direct

402 decomposition to H_2O and to trace amounts of $O_{2(aq)}$, when compared to conditions prior

403 to $O_{2(aq)}$ elimination. This is in agreement with previous observations (CHINTA and

404 LUNSFORD, 2004; LANDON et al., 2003; POSPELOVA et al., 1961). Here, H_2O radiolysis

405 has been proposed to support communities of thermophilic H_2-utilizing and sulfate

406 reducing bacteria, without any apparent mechanism to allow removal of the oxidant

407 radiolysis byproducts (e.g. H_2O_2) (LIN et al., 2005; LIN et al., 2006). The strong effect of

408 $H_{2(aq)}$ in enhancing H_2O_2 decomposition under anaerobic conditions, as observed in our

409 experiments, could potentially serve this role and in this way reduce oxidative stress for

410 organisms living in such deep crustal fractures, in line with genomic data indicating a

411 limited machinery to cope with oxidative stress (CHIVIAN et al., 2008).

412   The counteracting oxidative effects of hydrogen peroxide occurrence under

413 reducing conditions is completely unknown and might alter the extent of the oxic-anoxic

414 zones developed during mixing of high-temperature anoxic hydrothermal fluid and cold

415 oxygenated seawater at near-seafloor environments. Experimental data showing

416 hydrothermal formation of $H_2O_{2(aq)}$ at temperatures and pressures typical of seafloor vent

417 environments could support the presence of dissolved $H_2O_{2(aq)}$ in low-temperature diffuse

418 fluids. In light of these results, we note that a number of hydrothermal vent bacteria,

419 encompassing obligate anaerobes, potentially living in this mixing zone have been shown

420 to have mechanisms to cope with oxidative stress, including the scavenging of

421 endogenous H_2O_2 (CAMPBELL et al., 2009; MARKERT et al., 2007; NAKAGAWA et al.,

422 2007; VETRIANI et al., 2004; VOORDECKERS et al., 2008).

423   The possibility of $H_2O_{2(aq)}$ coexisting with Fe-oxides or dissolved Fe^{+2} at seafloor

424 hydrothermal vents, could also provide a suitable catalytic substrate to promote formation

425 of hydroxyl radicals (•OH). Possible reactions that facilitate radical formation in place of

426 a non-radical $H_2O_{2(aq)}$ decomposition to $O_{2(aq)}$ and H_2O (Eq. 1), are closely related to the

427 general scheme of Fenton-type chemistry (KWAN and VOELKER, 2003):

428 $$Fe^{+2} + H_2O_{2(aq)} \rightarrow Fe^{+3} + OH^- + \bullet OH \qquad (6)$$
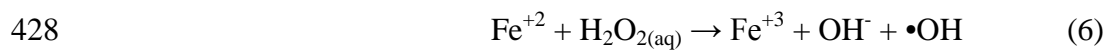
429 This is a well-known reaction used extensively in environmental engineering for

430 wastewater remediation, where formation of •OH enables the chemical oxidation of

431 organic contaminants. While the reaction commonly involves Fe^{+2} dissolved in solution,

432 magnetite has been shown to be the most catalytically effective Fe-oxide reactant, mainly

433 due to coexistence of Fe^{+2} and Fe^{+3} on the octahedral sites of the mineral lattice (COSTA

434 et al., 2006; MOURA et al., 2006). A recent experimental study has indeed demonstrated

435 the role of magnetite-catalyzed Fenton reaction in promoting $H_2O_{2(aq)}$ decomposition and

436 hydroxyl radical formation under low temperature hydrothermal conditions (80-150 $^{\circ}C$;

437 172-241 bar) (FOUSTOUKOS AND STERN, 2010). Undoubtedly, the likelihood of dissolved

438 hydroxyl radicals being stable in diffuse flow fluids, when coexisting with Fe-oxides, has

439 important implications for a number of geochemical and biochemical processes occurring

440 in near-seafloor hydrothermal sites. Fluxes of such strong oxidants (e.g. H_2O_2, •OH) will

441 impose significant constraints on redox conditions in seawater/hydrothermal fluid

442 mixtures, affecting not only the kinetic rates of homogeneous $H_{2(aq)}$ oxidation, but also

443 the distribution of dissolved alkanes and carboxylic acids in diffuse flow hydrothermal

444 vent fluids. This process may be important in decreasing the flux of dissolved organic

445 carbon (DOC) in low-temperature vent fluids, and thus, serve as a plausible mechanism

446 to explain the DOC-depleted diffuse fluids sampled at Bay Bare Seamount and ODP

447 Hole 1026B; off-axis sites near Juan de Fuca Ridge (LANG et al., 2006).

448

449 **5. Conclusions**

450 We conducted a series of open and closed system experiments utilizing flow-

451 though and flexible Au/Ti reaction cells to examine the effect of temperature on $H_{2(aq)}$-

452 $O_{2(aq)}$ equilibria. These experiments involved mixing of $H_{2(aq)}$- and $O_{2(aq)}$-bearing aqueous

453 solutions at temperature and pressure conditions reflecting near-seafloor hydrothermal

454 environments (55-250 ^{o}C and 242-497 bar). This fundamental redox equilibria expressed

455 through the Knallgas reaction has been shown to proceed instantaneously to

456 thermodynamic equilibrium at elevated temperatures and pressures (SEEWALD, 1994).

457 Results in our experiments, however, revealed that $H_{2(aq)}$ oxidation is inhibited as

458 temperature decreases, allowing for development of excess $H_{2(aq)}$ in solution and, most

459 importantly, promoting the stability of hydrogen peroxide as a metastable intermediate

460 phase evolving along the reaction pathway for water formation.

461 The slow reaction rate of $H_{2(aq)}$-$O_{2(aq)}$ redox equilibrium and the synthesis of

462 hydrogen peroxide at low temperatures may influence the oxidation of dissolved organic

463 species in an unpredictable way. For example, the relatively sluggish rate of oxidation of

464 short-chain alkanes predicted for low temperature chemical alteration can be overturned

465 by the oxidation effects of such a strong oxidant. Thus, formation of hydrogen peroxide

466 during H_2-O_2-H_2O disequilibria at temperatures lower than 130^oC suggests that the

467 oxidation of alkanes could occur under hydrothermal conditions, providing a possible

468 mechanism to produce molecules that have relevance for prebiotic chemistry, such as

469 methanol and formaldehyde that serve as intermediates during methane oxidation to CO_2

470 and CO. Formation of these metastable phases at low temperatures will provide new

471 insights on the availability of complex organic compounds in hydrothermal environments

472 and impose important constraints on the habitability of other planetary bodies containing

473 liquid water.

474

Table 1. Distribution of dissolved H_2 and $O_{2(aq)}$ in fluid samples retrieved from hydrothermal experiments at 100 $^{\circ}$C and 500 bar (Houghton, 2003).

Reaction time (hrs)	$H_{2aq)}$ (mmol/kg)	$O_{2aq)}$ (mmol/kg)	Rate constant (k_{H2}) (s^{-1})
0	2.012	1.104	$5.45 \times 10^{-5} \pm 1.7 \times 10^{-6}$
0.5	1.443	0.809	$r^2 = 0.84$
2	0.976	0.023	
4	0.865	n.d.	

Table 2. Results of flow-through experiments on $H_2O_{2(aq)}$ decomposition at 60-200 ^{o}C and 242 bar.

Fluid flow rate (ml/min)	Reaction time (sec)	$H_2O_{2(aq)}$ (mmol/kg)	2σ [a] (mmol/kg)	Rate constant (k) (s^{-1})
T = 60 ^{o}C				$5.77 \times 10^{-5} \pm 2.310^{-5}$
start		1.995	0.02	$r^2 = 0.47$
0.66	310	1.752	0.02	
0.66	310	1.845	0.02	
0.33	621	1.686	0.02	
0.33	621	1.845	0.02	
0.22	931	1.799	0.02	
0.22	931	1.750	0.02	
0.11	1862	1.656	0.02	
0.11	1862	1.732	0.02	
T = 90 ^{o}C				$2.48 \times 10^{-4} \pm 6.9 \times 10^{-5}$
start		1.092	0.012	$r^2 = 0.72$
0.685	299	1.010	0.016	
0.685	299	1.032	0.012	
0.228	898	0.666	0.012	
0.228	898	0.860	0.012	
0.114	1796	0.733	0.012	
0.114	1796	0.673	0.012	
T = 120 ^{o}C				$1.43 \times 10^{-3} \pm 5.8 \times 10^{-5}$
start		1.995	0.02	$r^2 = 0.99$
0.66	310	1.255	0.02	
0.66	310	1.415	0.061	
0.33	621	1.108	0.015	
0.33	621	1.065	0.063	
0.22	931	0.545	0.02	
0.22	931	0.677	0.02	
0.11	1862	0.159	0.02	
T = 150 ^{o}C				$2.11 \times 10^{-3} \pm 2.3 \times 10^{-4}$
start		1.092	0.012	$r^2 = 0.95$
1.37	149	0.853	0.012	
0.685	299	0.583	0.012	
0.685	299	0.591	0.012	
0.342	599	0.363	0.04	
0.342	599	0.290	0.04	
T = 180 ^{o}C				$4.29 \times 10^{-5} \pm 3.3 \times 10^{-4}$
start		1.995	0.02	$r^2 = 0.98$
1.32	155	0.951	0.02	
1.32	155	0.913	0.02	
0.66	310	0.545	0.02	
0.66	310	0.479	0.02	

T = 200 $^{\circ}$C				5.51×10^{-3} $\pm 3.1 \times 10^{-4}$
start		1.092	0.012	$r^2 = 0.99$
1.32	155	0.951	0.02	
1.32	155	0.913	0.02	
0.66	310	0.545	0.02	
0.66	310	0.479	0.02	

[a] Analytical errors reported are the larger values of errors associated with instrument calibration and duplicate analysis of individual samples.

The volume of the titanium reactor, including tubing situated within the high temperature zone, is 3.413 ml.

483

Table 3. Concentrations of dissolved $H_{2(aq)}$ and $H_2O_{2(aq)}$ measured in samples collected during flow-through experiments on H_2 oxidation at 200-250 ^{o}C and 242 bar.

	Fluid flow rate (ml/min)	Reaction time (sec)	$H_{2aq)}$ (mmol/kg)	$H_2O_{2(aq)}$ (mmol/kg)	2σ [a] (mmol/kg)	pH (25 ^{o}C)	Rate constant (k_{H2}) (s^{-1})
T = 200 ^{o}C							$4.11 \times 10^{-4} \pm 4.0 \times 10^{-5}$
start (25 ^{o}C)	2	102	0.638	2.249	0.009	5.9	r^2 = 0.93
start (25 ^{o}C)	2	102	0.646	2.341	0.009	6.0	
	2	102	0.596	1.136	0.012	6.0	$k_{H2O2} = 1.63 \times 10^{-2} \pm 8.5 \times 10^{-3}$
	0.678	300	0.515	0.079	0.007	6.6	r^2 = 0.55
	0.678	300	0.549	0.061	0.001	6.1	
	0.678	300	0.542	0.021	0.007	6.5	
	0.226	900	0.435	b.d.		6.4	
	0.226	900	0.456	b.d.		5.8	
	0.226	900	0.426	b.d.		6.2	
	0.226	900	0.455	b.d.		6.2	
T = 250 ^{o}C							$5.35 \times 10^{-4} \pm 3.2 \times 10^{-5}$
start (25 ^{o}C)	2	102	0.638	2.410	0.033	6.0	r^2 = 0.98
start (25 ^{o}C)	2	102	0.627	2.495	0.035	6.2	
	2	102	0.602	0.205	0.014	6.3	$k_{H2O2} = 1.71 \times 10^{-2} \pm 4.3 \times 10^{-3}$
	2	102	0.605	0.212	0.024	6.2	r^2 = 0.76
	0.685	297	0.514	n.a.		6.5	
	0.685	297	0.499	0.019	0.029	6.5	
	0.685	297	0.541	0.005	0.008	6.3	
	0.228	892	0.380	b.d.		6.6	
	0.228	892	0.398	b.d.		6.7	
	0.228	892	0.391	b.d.		6.4	

[a] Analytical errors reported are the larger values of errors associated with instrument calibration and duplicate analysis of individual samples.

Errors for dissolved $H_{2(aq)}$ analysis are $\pm$ 5%. The volume of the titanium reactor, including tubing situated within the high temperature zone, is 3.390 ml.

b.d.: below detection limit

n.a.: not analyzed

Table 4. Concentrations of dissolved aqueous species during H_2 oxidation in closed system hydrothermal experiments at 55-130 °C and 297-497 bar.

	P (bar)	Reaction time (min)	$H_{2(aq)}$ (mmol/kg)	$O_{2(aq)}$ (mmol/kg)	$H_2O_{2(aq)}$ (mmol/kg)	2σ [a] (mmol/kg)	pH (25 °C)	Cl [c] (ppm)	Rate constant (k_{H2}) (s⁻¹)
T = 55 °C									$2.69 \times 10^{-5} \pm 3.2 \times 10^{-6}$
start					8.00	0.04	5.8	15	$r^2 = 0.94$
	234	874		4.00[b]	b.d.		6.1		
	299	895		4.00[b]	b.d.		5.8		
Injection of aqueous solution containing 32 mmol/kg $H_{2(aq)}$ – Final concentration of 4.45 mmol/kg									
	326	92	3.99	3.44[b]	b.d.		6.7		
	299	135	3.84	n.a	b.d.		6.8	42	
	276	185	3.01	n.a	b.d.		6.6		
	315	241	2.89	n.a	b.d.		6.3		
	308	347	2.43	n.a	b.d.		6.2	37	
	276	427	2.40	n.a	b.d.		6.3		
T = 130 °C									$7.63 \times 10^{-5} \pm 1.1 \times 10^{-5}$
start					7.92	0.04	5.0	16	$r^2 = 0.89$
	411	110		3.96[b]	b.d.				
Injection of aqueous solution containing 32 mmol/kg $H_{2(aq)}$ – Final concentration of 4.51 mmol/kg									
	307	47	3.15	3.40[b]	0.008	0.0002	5.6	28	
	355	62	2.86	n.a	0.012	0.0003	5.6		
	335	92	2.62	n.a	0.008	0.0002	5.7		
	328	107	2.17	n.a	0.018	0.0003	5.4		
	320	122	2.77	n.a	0.015	0.0002	5.5	27	
	302	152	2.11	n.a	0.010	0.0002	5.6	32	
	329	182	1.77	n.a	0.009	0.0002	5.4		
T = 125 °C									$1.89 \times 10^{-4} \pm 4.3 \times 10^{-6}$
start					12.39	0.12	4.5		$r^2 = 0.99$
	397	133		5.86	b.d.		6.0	13	
	383	139		5.94	b.d.				
Injection of aqueous solution containing 40 mmol/kg $H_{2(aq)}$ – Final concentration of 5.9 mmol/kg									
	424	42	4.61	4.23	0.113	0.0004	5.9		
	435	57	2.54	2.92	0.110	0.0003	6.0		
	401	68	2.76	3.32	0.124	0.0009	6.1		
	393	87	2.04	2.80	0.077	0.0003	n.a	34	
	343	129	1.31	2.41	0.051	0.0007	6.0		
	450	157	0.965	2.04	0.038	0.0003	n.a		
	364	184	0.677	2.32	0.025	0.0002	5.9		
	395	213	0.480	2.13	0.029	0.0002	6.0		
	402	242	0.337	1.84	0.006	0.0002	6.0		
	391	291	0.245	1.71	0.008	0.0002	5.7	28	
	397	335	0.129	2.21	0.005	0.0002	5.9		
	355	391	0.060	1.66	b.d.		n.a		
	329	421	0.058	2.14	b.d.		n.a		

T = 95 °C						$4.37 \times 10^{-5} \pm 3.7 \times 10^{-6}$
start			11.81	0.12	4.7	$r^2 = 0.94$
499	171	4.85	b.d.		5.6	11
468	184	4.82	b.d.			

Injection of aqueous solution containing 53 mmol/kg $H_{2(aq)}$ – Final concentration of 8.0 mmol/kg

497	50	7.46	4.48	0.064	0.0008	6.0	
450	79	6.43	3.86	0.123	0.0002	6.0	
456	105	5.19	3.28	0.154	0.0011	5.9	36
439	134			0.149	0.0004	n.a	
458	149	5.42	3.36	0.154	0.0010	5.9	
457	182	5.06	3.24	0.172	0.0010	5.8	
409	211	4.22	2.85	0.148	0.0002	n.a	
412	240	4.55	3.09	0.145	0.0002	5.9	28
428	252	4.05	2.65	0.147	0.0004	n.a	33
403	289	3.47	2.48	0.156	0.0002	6.0	
419	322	3.57	2.71	0.118	0.0002	5.9	
440	360	2.27	1.88	0.100	0.0008	5.9	
411	1426	0.388	1.33	0.013	0.0003	n.a	
389	1451	0.365	1.22	0.011	0.0002	6.7	35

Injection of aqueous solution containing 45 mmol/kg $H_{2(aq)}$ – Final concentration of 8.16 mmol/kg

471	29	8.73	0.44	0.047	0.0004	6.8	
435	110	3.68	0.42	0.048	0.0002	n.a	
411	123	4.46	0.10	0.036	0.0002	6.9	67
428	154	6.46		0.003	0.0001	6.7	64
447	163	5.40		b.d.		n.a	

---

[a] Analytical errors reported are the larger values of errors associated with instrument calibration and duplicate analysis of individual samples. Errors for dissolved $H_{2(aq)}$ and $O_{2(aq)}$ analysis are $\pm 5\%$. Oxygen compositions have been adjusted to account for contributions from atmospheric O_2.

[b] Dissolved O_2 concentrations estimated assuming complete decomposition of $H_2O_{2(aq)}$

[c] Dissolved chloride concentration in the injected aqueous solution is 176 ppm. Fluids were spiked with chloride to better constrain final mixing ratios in the batch reactor, and estimate the dissolved H_2 concentrations attained immediately after injection of the H_2-bearing aqueous solutions.
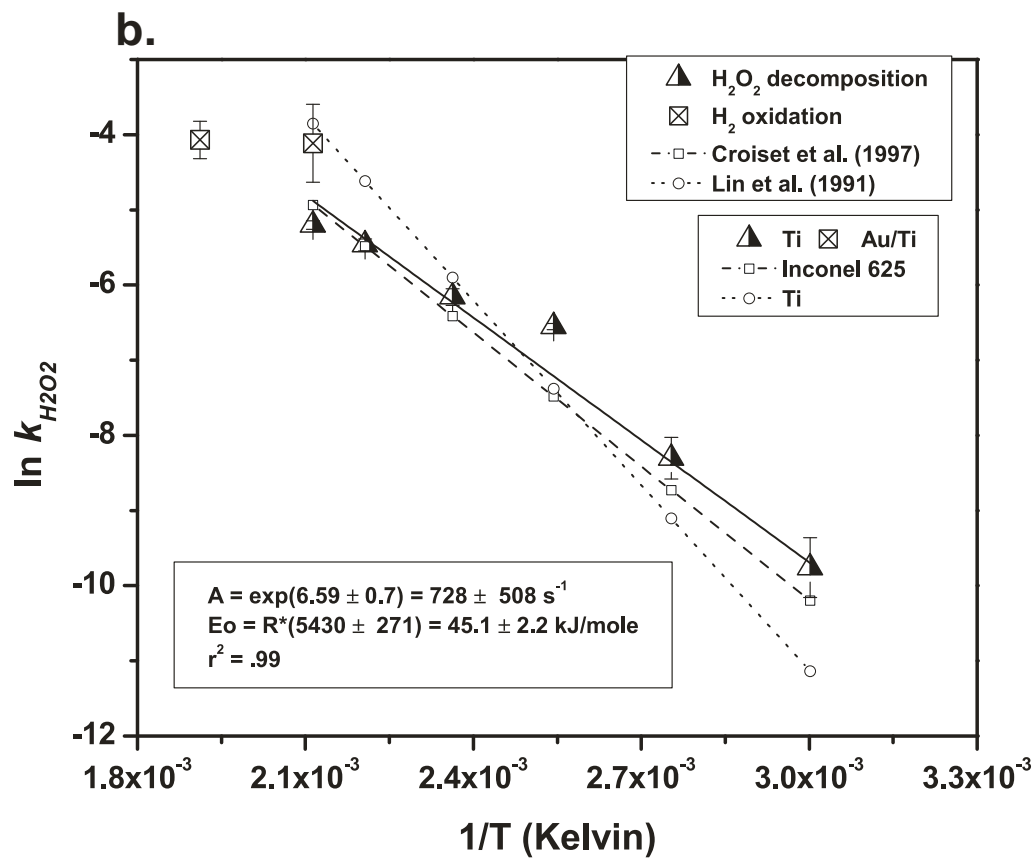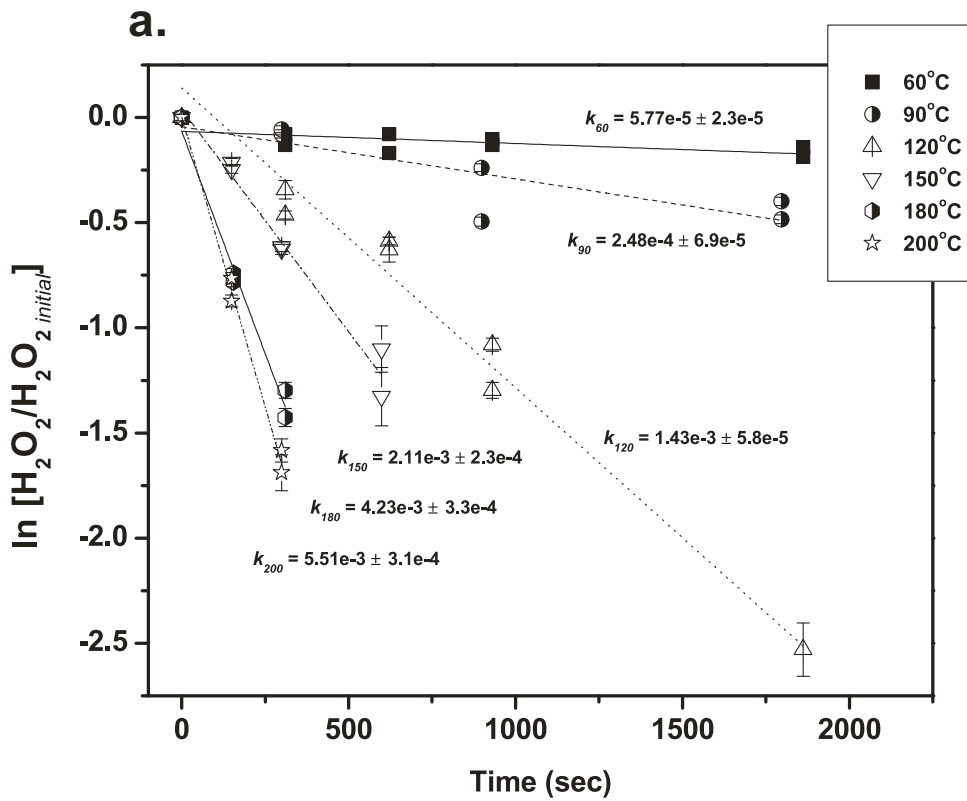
b.d.: below detection limit

n.a.: not analyzed

484
485
486

487

**a.**

Legend:
- ■ 60°C
- ◐ 90°C
- △ 120°C
- ▽ 150°C
- ◐ 180°C
- ☆ 200°C

$k_{60} = 5.77e\text{-}5 \pm 2.3e\text{-}5$

$k_{90} = 2.48e\text{-}4 \pm 6.9e\text{-}5$

$k_{120} = 1.43e\text{-}3 \pm 5.8e\text{-}5$

$k_{150} = 2.11e\text{-}3 \pm 2.3e\text{-}4$

$k_{180} = 4.23e\text{-}3 \pm 3.3e\text{-}4$

$k_{200} = 5.51e\text{-}3 \pm 3.1e\text{-}4$

y-axis: $\ln [H_2O_2/H_2O_{2\,initial}]$

x-axis: Time (sec)

b.

Legend:
- ▲ H_2O_2 decomposition
- ⊠ H_2 oxidation
- -□- Croiset et al. (1997)
- ○ Lin et al. (1991)

- ▲ Ti ⊠ Au/Ti
- -□- Inconel 625
- ○ Ti

$A = \exp(6.59 \pm 0.7) = 728 \pm 508\ s^{-1}$

$E_o = R^*(5430 \pm 271) = 45.1 \pm 2.2\ kJ/mole$

$r^2 = .99$

y-axis: $\ln k_{H2O2}$

x-axis: 1/T (Kelvin)

488

489   Figure 1. Decomposition of $H_2O_{2(aq)}$ in the homogeneous H_2O_2-H_2O system at 60-200 ^{o}C

490   and 242 bar. (a) Experimental data indicate first-order reaction rate supported by the

491   linear correlation between the natural logarithm values of $H_2O_{2(aq)}$ concentrations and

492   reaction time. The slope of the line defines the kinetic rate constant (k_{H2O2}) at a range of

493   temperatures, and allows temperature-dependent decay rates to be described in an

494   Arrhenius plot (b). Results are in good agreement with previous studies of H_2O_2

495   decomposition that involved titanium and Inconel 625 reactors. Furthermore, rates of

496   H_2O_2 decay in the H_2-enriched experiments conducted by utilizing a flexible Au/Ti

497   reaction cell at temperatures of 200-250 ^{o}C (Table 3), are consistent with the kinetic rate

498   law constants (A, E_a) determined from the lower temperature experimental data.

499

500

a.

b.
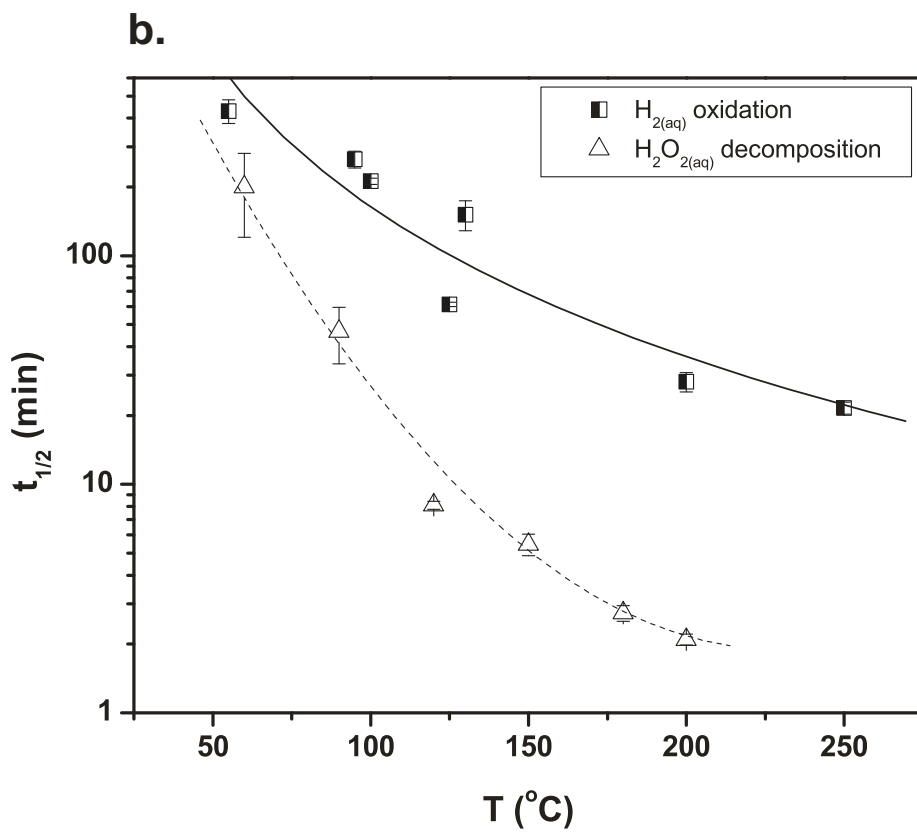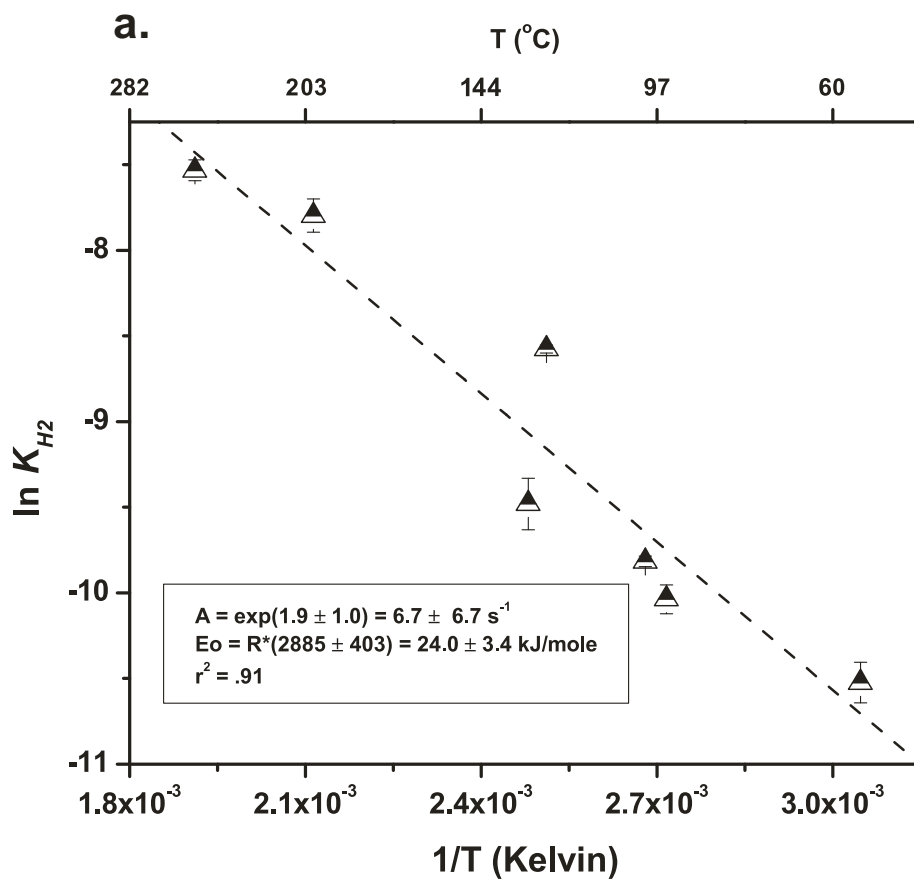
502   Figure 2. Arrhenius plot and rate constants of H_2 oxidation in presence of dissolved $O_{2(aq)}$

503   at temperatures ranging from 55°C to 250°C and pressures of 242 - 497 bar. (a). The first

504   order temperature-dependent oxidation rate of $H_{2(aq)}$ is described with an activation

505   energy (E_a) of 24 $\pm$ 3.4 kJ/mole and an pre-exponential factor (A) of 6.7 $\pm$ 6.7 s^{-1},

506   resulting in reaction half-times that range from 22 minutes to 430 minutes at 250°C and

507   55°C respectively. Arrhenius parameters also include the kinetic rate constant measured

508   at 100°C – 500 bar by Houghton (2003) (Table 1). (b). Experimental observations and

509   model results provide evidence of strong H_2-O_2 disequilibrium at low temperatures that

510   allows excess $H_{2(aq)}$ and establishment of highly reducing conditions. Estimated half-life

511   of $H_2O_{2(aq)}$ decay is nearly an order of magnitude lower than that of $H_{2(aq)}$ oxidation and is

512   approximately 200 and 2 min at 60°C and 200°C, respectively.

513
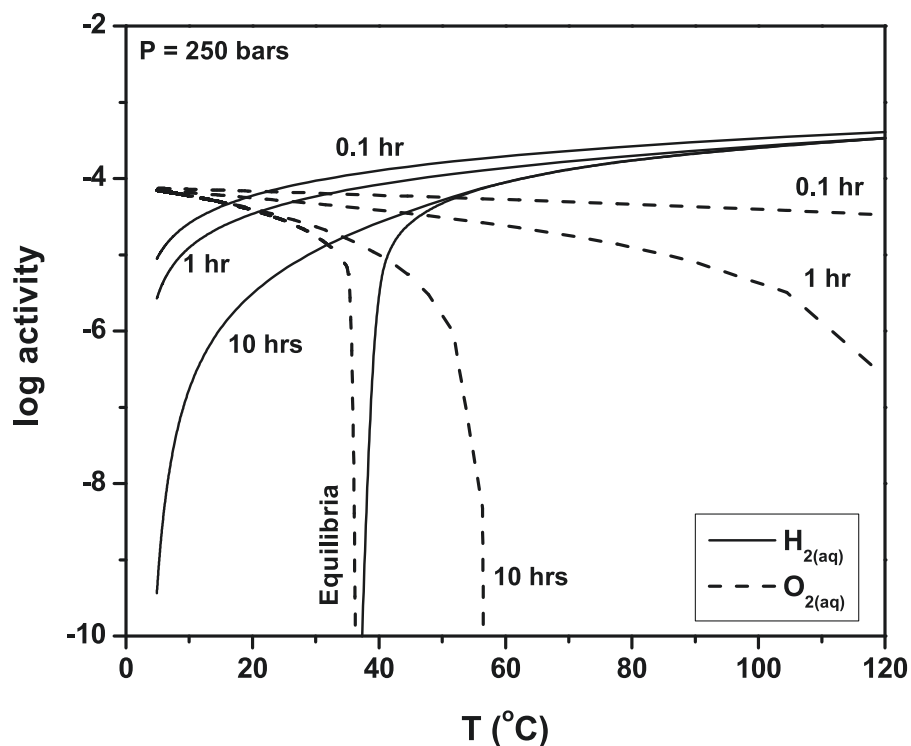
Figure 3. Theoretical modeling of the distribution of $H_{2(aq)}$ and $O_{2(aq)}$ during mixing between high-temperature $H_{2(aq)}$-enriched hydrothermal fluid and oxygenated seawater, performed with compositional constraints described by McCollom and Shock (1997), while utilizing the experimentally derived kinetic rate of H_2 oxidation from the present study. Equilibrium conditions develop a sharp redox gradient at 38°C, in agreement with previous studies (MCCOLLOM and SHOCK, 1997). Mixing processes occurring at different residence times (0.1-10 hrs), however, reveal formation of fluids highly enriched in both $H_{2(aq)}$ and $O_{2(aq)}$ at a range of temperatures, weakening the presence of a sharp oxic/anoxic interface. This, in turn, might have important implications for the distribution of anaerobic, microaerophilic and aerobic chemolithoautotrophs at diffuse flow vent sites and within near-vent subsurface environments by allowing for enhanced microbial diversity at a wide range of temperature and redox conditions.
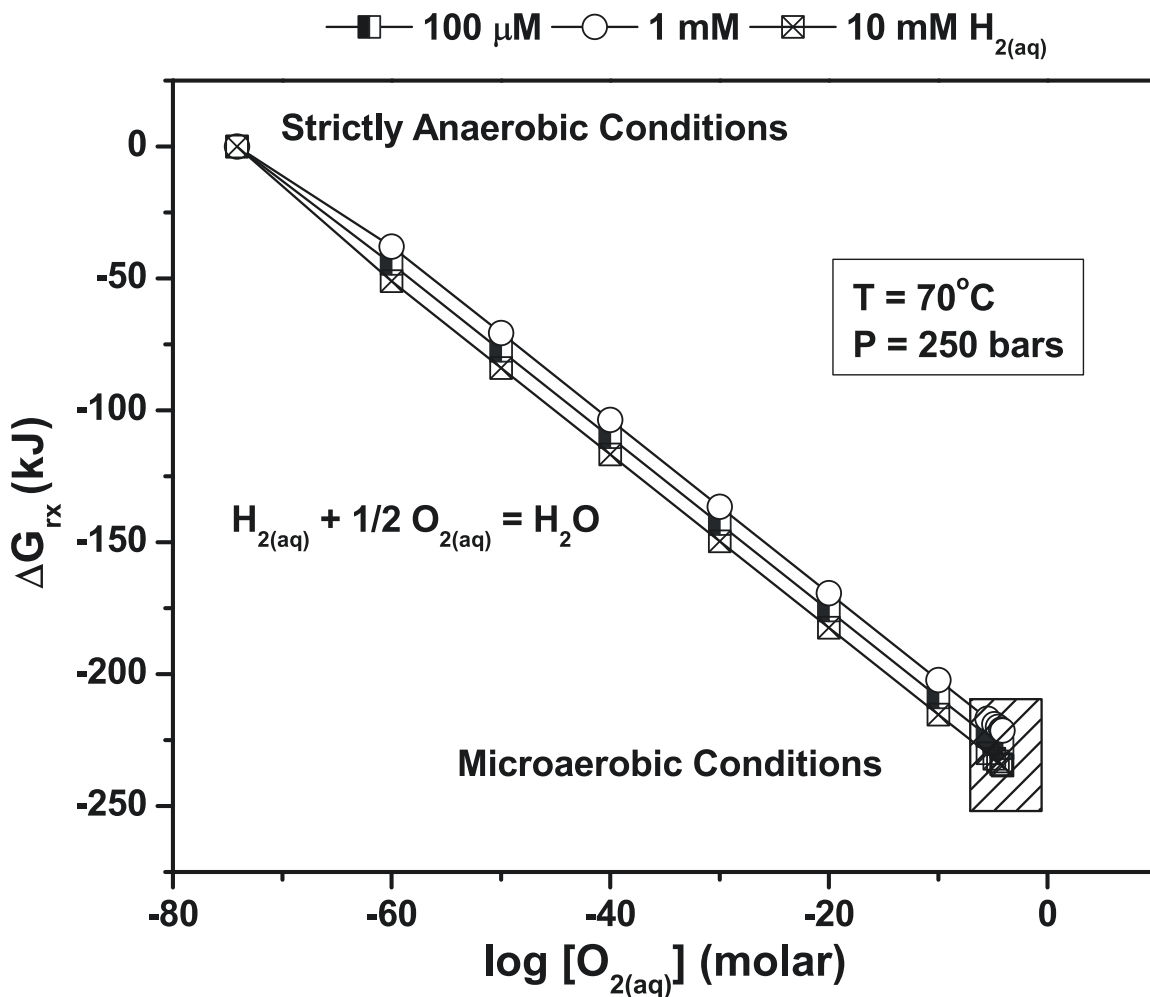
Figure 4. Energetics of the Knallgas reaction as function of available $O_{2(aq)}$ in solution.

Under equilibrium conditions, abundant presence of $H_{2(aq)}$ at concentrations ranging from

100 μM to 100 mM results in strictly anaerobic conditions. The presence of microaerobic

$O_{2(aq)}$ concentrations reflecting the tolerance limits of NO_3-reducers (2 - 54 μM) (shaded

box), however, has a great affinity to provide bioavailable energy at levels that permit

respiratory denitrification to be more favorable over ammonification. Thus, the

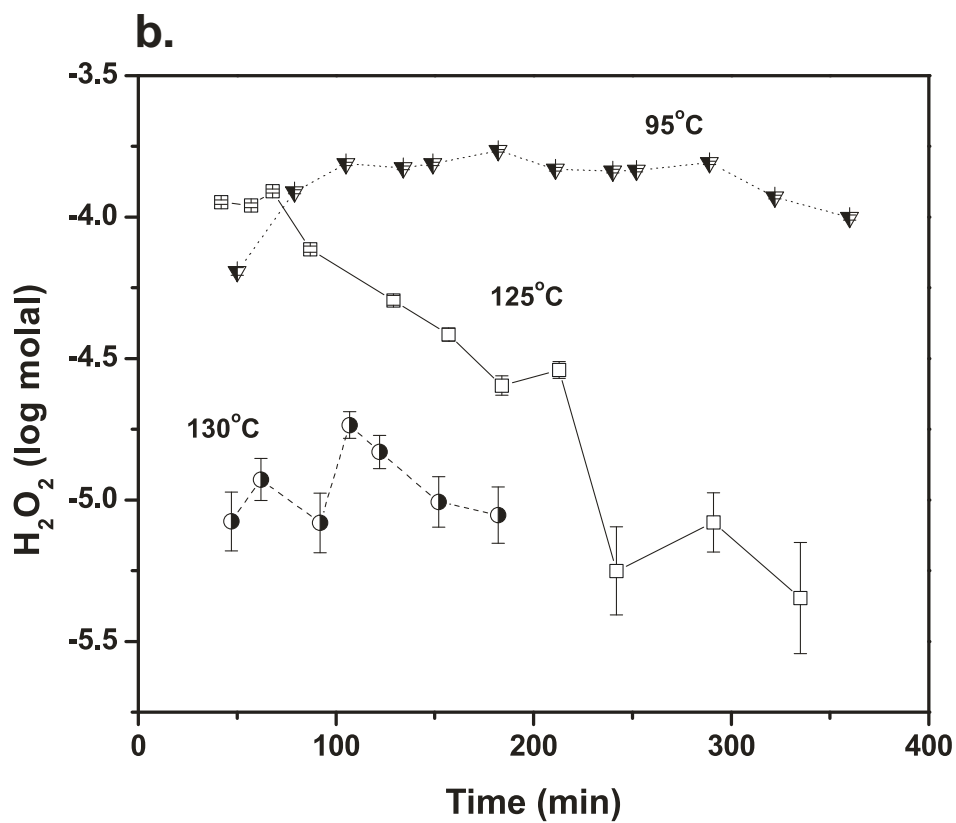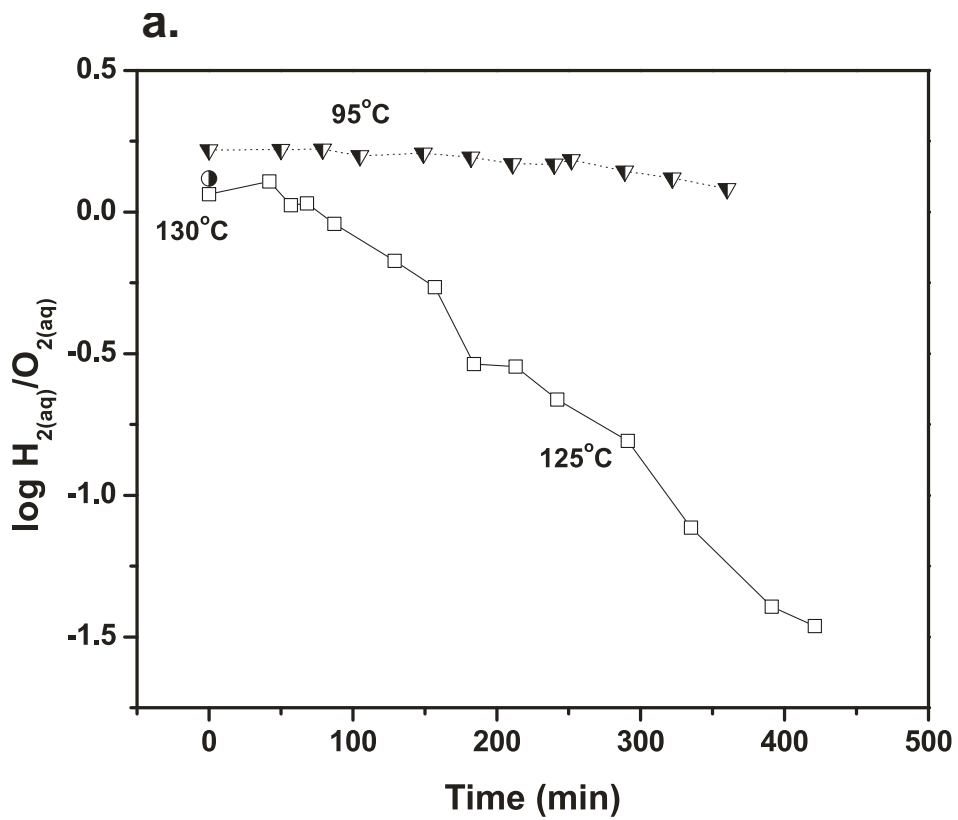adaptability of anaerobic microorganisms to utilize trace amounts of $O_{2(aq)}$ might greatly

affect microbial diversity at subsurface habitats as it can control metabolic pathways (e.g.

denitrification vs ammonification) developed along complex and dynamic redox

gradients. Gibbs energy calculations for the Knallgas reaction were performed following

537 methodologies discussed in other theoretical studies (MᶜCᴏʟʟᴏᴍ and Sʜᴏᴄᴋ, 1997;

538 Sʜᴏᴄᴋ and Hᴏʟʟᴀɴᴅ, 2004).

a.

95°C

130°C

125°C

b.

95°C

125°C

130°C

539
540

541   Figure 5. Experimental results of metastable $H_2O_{2(aq)}$ formation under elevated H_2/O_2

542   molar ratios and temperatures between 95 ^{o}C and 130 ^{o}C (242-497 bar). Dissolved

543      $H_2O_{2(aq)}$ concentrations attained values (0.002 – 0.156 mmol/kg) significantly higher than

544   those predicted based on rates of direct H_2O_2 decomposition to H_2O and $O_{2(aq)}$. The yield

545   of $H_2O_{2(aq)}$ is dependent on both $H_{2(aq)}$ and $O_{2(aq)}$ concentrations. However, highly

546   reducing conditions appear to increase the extent of metastable equilibria between H_2, O_2

547   and H_2O_2. Under these conditions, direct decomposition of hydrogen peroxide is

548   suppressed and the $H_2O_{2(aq)}$ hydrogenation to H_2O might have reached a steady-state

549   condition likely due to the presence of highly enriched $H_{2(aq)}$ solutions. This is clearly

550   demonstrated at 95 ^{o}C, where elevated H_2/O_2 molar ratios were sustained for reaction

551   times of nearly 24 hrs.
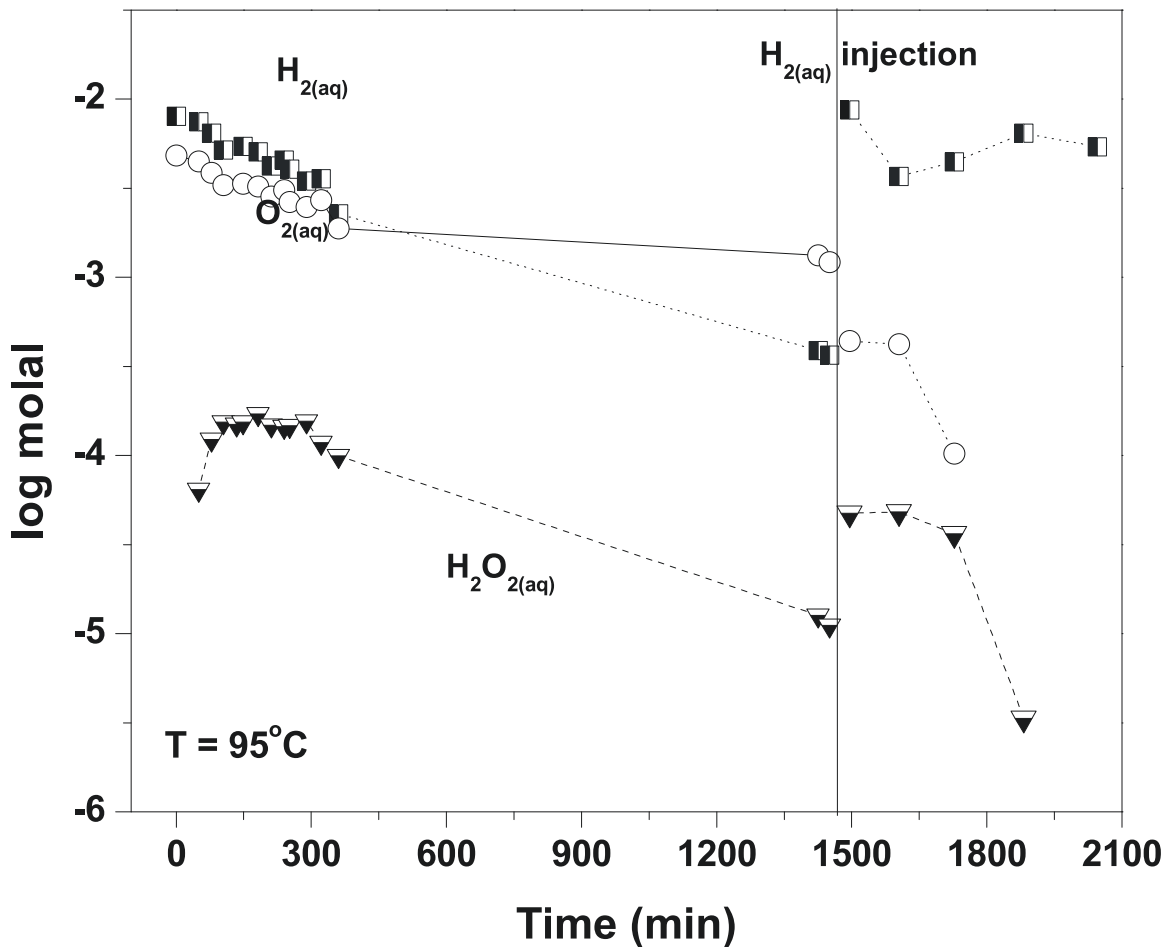
Figure 6. The catalytic effect of elevated $H_{2(aq)}/O_{2(aq)}$ ratios on enhancing synthesis of

H_2O_2 at low temperature hydrothermal conditions. Injection of $H_{2(aq)}$ in the Au/Ti

reaction cell after nearly 24 hrs of H_2 oxidation at 95 ^{o}C resulted in a significant increase

in dissolved $H_2O_{2(aq)}$ concentrations, supporting the effect of elevated $H_{2(aq)}/O_{2(aq)}$ on the

yield of dissolved oxidants. Furthermore, results are indicative of kinetically favored

H_2O_2 decomposition through the reaction pathway involving hydrogenation to H_2O based

on the elimination of $H_2O_{2(aq)}$ observed after $O_{2(aq)}$ removal from solution. In effect, this

might have implications for the habitability of deep crustal environments controlled by

the distribution of H_2O radiolysis products (e.g. H_2, H_2O_2, OH radicals) and the

availability of electron donors for anaerobic metabolism (e.g. H_2), such as the volcanic

units in the Witwatersrand Basin, South Africa.

564

REFERENCES

566

Alain, K., Querellou, J., Lesongeur, F., Pignet, P., Crassous, P., Raguenes, G., Cueff, V., and Cambon-Bonavita, M. A., 2002. *Caminibacter hydrogeniphilus* gen. nov., sp nov., a novel thermophilic, hydrogen-oxidizing bacterium isolated from an East Pacific Rise hydrothermal vent. *Int. J. Syst. Evol. Microbiol.* **52**, 1317-1323.

Balk, M., Bose, M., Ertem, G., Rogoff, D. A., Rothschild, L. J., and Freund, F. T., 2009. Oxidation of water to hydrogen peroxide at the rock-water interface due to stress-activated electric currents in rocks. *Earth Planet. Sci. Lett.* **283**, 87-92.

Bethke, C. M., 1996. *Geochemical reaction modeling: Concepts and applications*. Oxford University Press, New York, 397 pp..

Bethke, C. M., 2002. *The Geochemist's WorkbenchTM, version 4.0, A User's Guide to Rxn, Act2, React, and Gtplot,* University of Illinois, Urbana, IL.

Borda, M. J., Elsetinow, A. R., Strongin, D. R., and Schoonen, M. A., 2003. A mechanism for the production of hydroxyl radical at surface defect sites on pyrite. *Geochim. Cosmochim. Acta* **67**, 935-939.

Butterfield, D. A., Lilley, M. D., Huber, J., Roe, K. K., Embley, R. W., and Massoth, G. J., 2004. Mixing, reaction and microbial activity in the sub-seafloor revealed by temporal and spatial variation in diffuse flow vents at axial volcano. In: Wilcock, W. S. D., DeLong, E. F., Kelley, D. S., Baross, J. A., and Cary, S. C. Eds.), *The Subsurface Biosphere at Mid-Ocean Ridges, AGU Monograph 144, pp. 269-289.*

Campbell, B. J., Engel, A. S., Porter, M. L., and Takai, K., 2006. The versatile epsilon-proteobacteria: key players in sulphidic habitats. *Nat. Rev. Microbiol.* **4**, 458-468.

Campbell, B. J., Smith, J. L., Hanson, T. E., Klotz, M. G., Stein, L. Y., Lee, C. K., Wu, D. Y., Robinson, J. M., Khouri, H. M., Eisen, J. A., and Cary, S. C., 2009. Adaptations to submarine hydrothermal environments exemplified by the genome of Nautilia profundicola. *Plos Genetics* **5**, e1000362, doi:10.1371/journal.pgen.1000362.

Chinta, S. and Lunsford, J., 2004. A mechanistic study of H_2O_2 and H_2O formation from H_2 and O_2 catalyzed by palladium in an aqueous medium. *J. Catal.* **225**, 249-255.

Chivian, D., Brodie, E.L., Alm, E.J., Culley, D.E., Dehal, P.S., DeSantis, t.Z., Gihring, T.M., Lapidus, A., Lin, L., and et al. 2008, Environmental genomics reveals a single-species ecosystem deep within Earth. *Science*, **322**, 275-278.

Choudhary, V. R. and Samanta, C., 2006. Role of chloride or bromide anions and protons for promoting the selective oxidation of H_2 by O_2 to H_2O_2 over supported Pd catalysts in an aqueous medium. *J. Catal.* **238**, 28-38.

Choudhary, V. R., Samanta, C., and Jana, P., 2007. Formation from direct oxidation of H-2 and destruction by decomposition/hydrogenation of H_2O_2 over Pd/C catalyst in aqueous medium containing different acids and halide anions. *Appl. Catal., A* **317**, 234-243.

Cohn, C. A., Simon, S. R., and Schoonen, M. A. A., 2008. Comparison of fluorescence-based techniques for the quantification of particle-induced hydroxyl radicals. *Part. Fibre Toxicol.* **5**, doi:10.1186/1743-8977-5-2.

608 Corliss, J. B., Dymond, J., Gordon, L. I., Edmond, J. M., Von Herzen, R. P., Ballard, R.
609   D., Green, K., Williams, D., Bainbridge, A., and et al., 1979. Submarine thermal
610   springs on the Galapagos Rift. *Science* **203**, 1073-83.
611 Costa, R. C. C., Lelis, M. F. F., Oliveira, L. C. A., Fabris, J. D., Ardisson, J. D., Rios, R.
612   R. V. A., Silva, C. N., and Lago, R. M., 2006. Novel active heterogeneous Fenton
613   system based on $Fe_{3-x}M_xO_4$ (Fe, Co, Mn, Ni): The role of M^{2+} species on the
614   reactivity towards H_2O_2 reactions. *J. Hazard. Mater.* **129**, 171-178.
615 Croiset, E., Rice, S. F., and Hanush, R., 1997. Hydrogen peroxide decomposition in
616   supercritical water. *AIChe* **43**, 2343-2352.
617 Davies, K. J. P., Lloyd, D., and Boddy, L., 1989. The effect of oxygen on denitrification
618   in Paracoccus-Denitrificans and Pseudomonas-Aeruginosa. *J. Gen. Microbiol.*
619   **135**, 2445-2451.
620 Ding, K., Seyfried, W. E., Jr., Tivey, M. K., and Bradley, A. M., 2001. In-situ
621   measurement of dissolved H_2 and H_2S in high-temperature hydrothermal vent
622   fluids at the main Endeavour Field, Juan de Fuca Ridge. *Earth Planet. Sci. Lett.*
623   **186**, 417-425.
624 Ding, K., Seyfried, W. E. J., Zhang, Z., Tivey, M. K., Von Damm, K. L., and Bradley, A.
625   M., 2005. The in-situ pH of hydrothermal fluids at mid-ocean ridges. *Earth*
626   *Planet. Sci. Lett.* **237**, 167-174.
627 Dissanayake, D. P. and Lunsford, J. H., 2002. Evidence for the role of colloidal
628   palladium in the catalytic formation of H_2O_2 from H_2 and O_2. *J. Catal.* **206**, 173-
629   176.
630 Dissanayake, D. P. and Lunsford, J. H., 2003. The direct formation of H_2O_2 from H_2 and
631   O_2 over colloidal palladium. *J. Catal.* **214**, 113-120.
632 Edmond, J. M., Measures, C., Mangum, B., Grant, B., Sclater, F. R., Collier, R., Hudson,
633   A., Gordon, L. I., and Corliss, J. B., 1979. On the formation of metal-rich deposits
634   at ridge crests. *Earth Planet. Sci. Lett.* **46**, 19-30.
635 Edwards, J. K., Carley, A. F., Herzing, A. A., Kiely, C. J., and Hutchings, G. J., 2008.
636   Direct synthesis of hydrogen peroxide from H_2 and O_2 using supported Au-Pd
637   catalysts. *Faraday Discuss.* **138**, 225-239.
638 Edwards, J. K., Solsona, B., N, E. N., Carley, A. F., Herzing, A. A., Kiely, C. J., and
639   Hutchings, G. J., 2009. Switching off hydrogen peroxide hydrogenation in the
640   direct synthesis process. *Science* **323**, 1037-1041.
641 Edwards, K. J., Bach, W., and McCollom, T., 2005. Geomicrobiology in oceanography:
642   microbe-mineral interactions at and below the seafloor. *Trends Microbiol.* **13**,
643   doi:10.1016/J.tim.2005.07.005.
644 Foustoukos, D. I. and Seyfried, W. E., 2007. Trace element partitioning between vapor,
645   brine and halite under extreme phase separation conditions. *Geochim.*
646   *Cosmochim. Acta* **71**, 2056-2071.
647 Foustoukos, D. I. and Stern, J.C. 2010. Oxidation of organics under hydrothermal
648   conditions: Implications for the evolution of methane on Mars, *Twelveth Annual*
649   *V. M. Goldschmidt Conference.* Knoxville, TN, #A302 (abstr.).
650 Foustoukos, D. I., Seyfried, W. E., Jr., Ding, K., and Pester, N. J., 2009. Dissolved
651   carbon species in associated diffuse and focused flow hydrothermal vents at the
652   Main Endeavour Field, northern Juan de Fuca ridge. *Geochem. Geophys. Geosyst.*
653   **10**, Q10003, doi:10.1029/2009GC002472.

Gomes, A., Fernandes, E., and Lima, J. L. F. C., 2005. Fluorescence probes used for detection of reactive oxygen species. *J. Biochem. Bioph. Methods* **65**, 45-80.

Gotz, D., Banta, A., Beveridge, T. J., Rushdi, A. I., Simoneit, B. R. T., and Reysenbach, A., 2002. *Persephonella marina* gen. nov., sp nov and *Persephonella guaymasensis* sp nov., two novel, thermophilic, hydrogen-oxidizing microaerophiles from deep-sea hydrothermal vents. *Int. J. Syst. Evol. Microbiol.* **52**, 1349-1359.

Gyulkhandanyan, A. V. and Pennefather, P. S., 2004. Shift in the localization of sites of hydrogen peroxide production in brain mitochondria by mitochondrial stress. *J. Neurochem.* **90**, 405-421.

Han, Y. F., Zhong, Z. Y., Ramesh, K., Chen, F. X., Chen, L. W., White, T., Tay, Q. L., Yaakub, S. N., and Wang, Z., 2007. Au promotional effects on the synthesis of H_2O_2 directly from H_2 and O_2 on supported Pd-Au alloy catalysts. *J. Phys. Chem. C* **111**, 8410-8413.

Hart, A. B., Mcfadyen, J., and Ross, R. A., 1963. Solid-oxide-catalyzed decomposition of hydrogen peroxide vapour. *Trans. Faraday Soc.* **59**, 1458-&.

Hernandez, D. and Rowe, J. J., 1987. Oxygen regulation of nitrate uptake in denitrifying Pseudomonas-Aeruginosa. *Appl. Environ. Microbiol.* **53**, 745-750.

Hiroki, A., Pimblott, S. M., and LaVerne, J. A., 2002. Hydrogen peroxide production in the radiolysis of water with high radical scavenger concentrations. *J. Phys. Chem. A* **106**, 9352-9358.

Hoare, D. E., Peacock, G. B., and Ruxton, G. R. D., 1967. Efficiency of surfaces in destroying hydrogen peroxide and hydroperoxyl radicals. *Tran. Faraday Soc.* **63**, 2498-&.

Houghton, J. L., 2003. Biogeochemistry of seafloor hydrothermal vent systems : an experimental study conducted at in situ conditions, PhD Thesis, University of Minnesota, MN, USA.

Hurowitz, J. A., Tosca, N. J., McLennan, S. M., and Schoonen, M. A. A., 2007. Production of hydrogen peroxide in Martian and lunar soils. *Earth Planet. Sci. Lett.* **255**, 41-52.

Kamei, G. and Ohmoto, H., 2000. The kinetics of reactions between pyrite and O_2-bearing water revealed from in situ monitoring of DO, Eh and pH in a closed system. *Geochim. Cosmochim. Acta* **64**, 2585-2601.

Kelley, D. S., Baross, J. A., and Delaney, J. R., 2002. Volcanoes, fluids, and life at mid-ocean ridge spreading centers. *Annu. Rev. Earth Planet. Sci.* **30**, 385-491.

Kwan, W. P. and Voelker, B. M., 2003. Rates of hydroxyl radical generation and organic compound oxidation in mineral-catalyzed Fenton-like systems. *Environ. Sci. Technol.* **37**, 1150-1158.

Landon, P., Collier, P. J., Carley, A. F., Chadwick, D., Papworth, A. J., Burrows, A., Kiely, C. J., and Hutchings, G. J., 2003. Direct synthesis of hydrogen peroxide from H_2 and O_2 using Pd and Au catalysts. *Phys. Chem. Chem. Phys.* **5**, 1917-1923.

Lang, S. Q., Butterfield, D. A., Lilley, M. D., Johnson, P., and Hedges, J. I., 2006. Dissolved organic carbon in ridge-axis and ridge-flank hydrothermal systems. *Geochim. Cosmochim. Acta* **15**, 3830-3842.

Lin, C. C., Smith, F. R., Ichikawa, N., Baba, T., and Itow, M., 1991. Decomposition of hydrogen peroxide in aqueous solutions at elevated temperatures. *Int. J. Chem. Kinet.* **23**, 971-987.

Lin, L. H., Hall, J., Lippmann-Pipke, J., Ward, J. A., Lollar, B. S., DeFlaun, M., Rothmel, R., Moser, D., Gihring, T. M., Mislowack, B., and Onstott, T. C., 2005. Radiolytic H_2 in continental crust: Nuclear power for deep subsurface microbial communities. *Geochem. Geophys. Geosyst.* **6**, Q07003, doi:10.1029/2004GC000907.

Lin, L. H., Wang, P. L., Rumble, D., Lippmann-Pipke, J., Boice, E., Pratt, L. M., Lollar, B. S., Brodie, E. L., Hazen, T. C., Andersen, G. L., DeSantis, T. Z., Moser, D. P., Kershaw, D., and Onstott, T. C., 2006. Long-term sustainability of a high-energy, low-diversity crustal biome. *Science* **314**, 479-482.

Lindberg, R. D. and Runnells, D. D., 1984. Groundwater redox reactions - an analysis of equilibrium state applied to Eh measurements and geochemical modeling. *Science* **225**, 925-927.

Lunsford, J. H., 2003. The direct formation of H_2O_2 from H_2 and O_2 over palladium catalysts. *J. Catal.* **216**, 455-460.

Luther, G. W., Glazer, B. T., Hohmann, L., Popp, J. I., Taillefert, M., Rozan, T. F., Brendel, P. J., Theberge, S. M., and Nuzzio, D. B., 2001. Sulfur speciation monitored in situ with solid state gold amalgam voltammetric microelectrodes: polysulfides as a special case in sediments, microbial mats and hydrothermal vent waters. *J. Environ. Monit.* **3**, 61-66.

Markert, S., Arndt, C., Felbeck, H., Becher, D., Sievert, S. M., Hugler, M., Albrecht, D., Robidart, J., Bench, S., Feldman, R. A., Hecker, M., and Schweder, T., 2007. Physiological proteomics of the uncultured endosymbiont of Riftia pachyptila. *Science* **315**, 247-250.

McCollom, T. M. and Seewald, J. S., 2006. Carbon isotope composition of organic compounds produced by abiotic synthesis under hydrothermal conditions. *Earth Planet. Sci. Lett.* **243**, 74-84.

McCollom, T. M. and Shock, E. L., 1997. Geochemical constraints on chemolithoautotrophic metabolism by microorganisms in seafloor hydrothermal systems. *Geochim. Cosmochim. Acta* **61**, 4375-4391.

McKenney, D. J., Drury, C. F., and Wang, S. W., 2001. Effects of oxygen on denitrification inhibition, repression, and derepression in soil columns. *Soil Sci. Soc. Am. J.* **65**, 126-132.

Miroshnichenko, M. L., L'Haridon, S., Schumann, P., Spring, S., Bonch-Osmolovskaya, E. A., Jeanthon, C., and Stackebrandt, E., 2004. Caminibacter profundus sp nov., a novel thermophile of Nautiliales ord. nov within the class 'Epsilonproteobacteria', isolated from a deep-sea hydrothermal vent. *Int. J. Syst. Evol. Microbiol.* **54**, 41-45.

Moura, F. C. C., Oliveira, G. C., Araujo, M. H., Ardisson, J. D., Macedo, W. A. A., and Lago, R. M., 2006. Highly reactive species formed by interface reaction between Fe-0-iron oxides particles: An efficient electron transfer system for environmental applications. *Appl. Catal. A* **307**, 195-204.

Nakagawa, S., Inagaki, F., Takai, K., Horikoshi, K., and Sako, Y., 2005a. Thioreductor micantisoli gen. nov., sp nov., a novel mesophilic, sulfur-reducing

chemolithoautotroph within the epsilon-Proteobacteria isolated from hydrothermal sediments in the Mid-Okinawa Trough. *Int. J. Syst. Evol. Microbiol.* **55**, 599-605.

Nakagawa, S. and Takai, K., 2008. Deep-sea vent chemoautotrophs: diversity, biochemistry and ecological significance. *FEMS Microbiol. Ecol.* **65**, 1-14.

Nakagawa, S., Takai, K., Horikoshi, K., and Sako, Y., 2003. Persephonella hydrogeniphila sp nov., a novel thermophilic, hydrogen-oxidizing bacterium from a deep-sea hydrothermal vent chimney. *Int. J. Syst. Evol. Microbiol.* **53**, 863-869.

Nakagawa, S., Takai, K., Inagaki, F., Horikoshi, K., and Sako, Y., 2005b. Nitratiruptor tergarcus gen. nov., sp nov and Nitratifractor salsuginis gen. nov., sp nov., nitrate-reducing chemolithoautotrophs of the epsilon-Proteobacteria isolated from a deep-sea hydrothermal system in the Mid-Okinawa Trough. *Int. J. Syst. Evol. Microbiol.* **55**, 925-933.

Nakagawa, S., Takaki, Y., Shimamura, S., Reysenbach, A. L., Takai, K., and Horikoshi, K., 2007. Deep-sea vent epsilon-proteobacterial genomes provide insights into emergence of pathogens. *Proc. Natl. Acad. Sci. USA* **104**, 12146-12150.

Pospelova, T. A. and Kobozev, N. I., 1961. Palladium catalyzed synthesis of hydrogen peroxide from the elements 2. The active centers of palladium in the synthesis of H_2O_2. *Zhurnal Fizicheskoi Khimii* **35**, 535-542.

Pospelova, T. A., Kobozev, N. I., and Eremin, E. N., 1961. Palladium catalyzed synthesis of hydrogen peroxide from the elements .1. Conditions for the formation of hydrogen peroxide. *Zhurnal Fizicheskoi Khimii* **35**, 298-305.

Reysenbach, A.-L., Banta, A. B., and Luther, G., 2000. Microbial essentials at vents. *Nature* **404**, 835.

Reysenbach, A.-L. and Shock, E., 2002. Merging genomes with geochemistry in hydrothermal ecosystems. *Science* **296**, 1077.

Schlitzer, R., 2000. Electronic atlas of WOCE hydrographic and tracer data now available. *Eos Trans. AGU* **81**, 45.

Seaver, L. C. and Imlay, J. A., 2001. Hydrogen peroxide fluxes and compartmentalization inside growing Escherichia coli. *J. Bacteriol.* **183**, 7182-7189.

Seaver, L. C. and Imlay, J. A., 2004. Are respiratory enzymes the primary sources of intracellular hydrogen peroxide? *J. Biol. Chem.* **279**, 48742-48750.

Seewald, J., 1994. Evidence for metastable equilibriuum between hydrocarbons under hydrothermal conditions. *Nature* **370**, 285-287.

Seewald, J. S., Zolotov, M. Y., and McCollom, T., 2006. Experimental investigation of single carbon compounds under hydrothermal conditions. *Geochim. Cosmochim. Acta* **70**, 446-460.

Seyfried, W. E. J., Janecky, D. R., and Berndt, M. E., 1987. Rocking autoclaves for hydrothermal experiments: II. The flexible reaction-cell system. In: H. Barnes and Ulmer, G. Eds.), *Hydrothermal Experimental Techniques*. Wiley-Interscience, New York.

Shock, E. L. and Holland, H. D., 2004. Geochemical energy sources that support the subsurface biosphere. In: Wilcock, W. S. D., DeLong, E. F., Kelley, D. S., Baross, J. A., and Cary, S. C. Eds.), *The Subsurface Biosphere at Mid-Ocean Ridges, AGU Monograph 144,* 153-165.

790   Strohm, T. O., Griffin, B., Zumft, W. G., and Schink, B., 2007. Growth yields in bacterial
791   denitrification and nitrate ammonification. *Appl. Environ. Microbiol.* **73**, 1420-
792   1424.
793   Takagi, J. and Ishigure, K., 1985. Thermal-decomposition of hydrogen-peroxide and its
794   effect on reactor water monitoring of boiling water-reactors. *Nuclear Sci. Eng.* **89**,
795   177-186.
796   Takai, K., Nealson, K. H., and Horikoshi, K., 2004. *Hydrogenimonas thermophila* gen.
797   nov., sp nov., a novel thermophilic, hydrogen-oxidizing chemolithoautotroph
798   within the epsilon-Proteobacteria, isolated from a black smoker in a Central
799   Indian Ridge hydrothermal field. *Int. J. Syst. Evol. Microbiol.* **54**, 25-32.
800   Takai, K., Suzuki, M., Nakagawa, S., Miyazaki, M., Suzuki, Y., Inagaki, F., and
801   Horikoshi, K., 2006. *Sulfurimonas paralvinellae* sp nov., a novel mesophilic,
802   hydrogen- and sulfur-oxidizing chemolithoautotroph within the Epsilonproteo-
803   bacteria isolated from a deep-sea hydrothermal vent polychaete nest,
804   reclassification of *Thiomicrospira denitrificans* as *Sulfurimonas denitrificans*
805   comb. nov and emended description of the genus Sulfurimonas. *Int. J. Syst. Evol.*
806   *Microbiol.* **56**, 1725-1733.
807   Tivey, M. K., 1995. The influence of hydrothermal fluid composition and advection rates
808   on black smoker chimney mineralogy: insights from modeling transport and
809   reaction. *Geochim. Cosmochim. Acta* **59**, 1933-49.
810   Vetriani, C., Speck, M. D., Ellor, S. V., Lutz, R. A., and Starovoytov, V., 2004.
811   *Thermovibrio ammonificans* sp nov., a thermophilic, chemolithotrophic, nitrate-
812   ammonifying bacterium from deep-sea hydrothermal vents. *Int. J. Syst. Evol.*
813   *Microbiol.* **54**, 175-181.
814   Voordeckers, J. W., Do, M. H., Hugler, M., Ko, V., Sievert, S. M., and Vetriani, C.,
815   2008. Culture dependent and independent analyses of 16S rRNA and ATP citrate
816   lyase genes: a comparison of microbial communities from different black smoker
817   chimneys on the Mid-Atlantic Ridge. *Extremophiles* **12**, 627-640.
818   Zhou, M., Diwu, Z., Panchuk-Voloshina, N., and Haugland, R., 1997. A stable
819   nonfluorescent derivative of resorufin for the fluorometric determination of trace
820   hydrogen peroxide: Applications in detecting the activity of phagocyte NADPH
821   oxidase and other oxidases. *Anal. Biochem.* **253**, 162-168.
822
823